

# Towards a Solid Earth Integrated Reference Frame

Stefania D.M. Wagenaar<sup>1</sup>, Bram Vaes<sup>2</sup>, Douwe J.J. van Hinsbergen<sup>1</sup>

<sup>1</sup>Department of Earth Sciences, Utrecht University, Budapestlaan 4, 3584 CD, Utrecht, the Netherlands

<sup>2</sup>Department of Earth and Environmental Sciences (DISAT), University of Milano-Bicocca, Piazza della Scienza 4, 20126, Milan, Italy

## Key Points:

- We construct a minimum continent velocity mantle reference frame and quantify uncertainty.
- Other parameters of plate-mantle interaction are coupled through the absolute plate model.
- This Solid Earth Integrated Reference Frame allows coupled hypothesis testing, reconstructing relative motions in the mantle, and training numerical models.

---

Corresponding author: Douwe van Hinsbergen, [D.J.J.vanHinsbergen@uu.nl](mailto:D.J.J.vanHinsbergen@uu.nl)

## 13 Abstract

14 Studying mantle convection requires knowledge of how plates moved over and subduct  
 15 into the mantle. Therefore, relative plate tectonic reconstructions are placed in a man-  
 16 tle reference frame. These use the geological expressions of plate-mantle interactions and  
 17 correlate these to mantle structure or minimize plate motions that would cause friction  
 18 with the mantle under the null hypothesis that active horizontal flow in the mantle is  
 19 negligible. However, mantle reference frames based on different plate-mantle interactions  
 20 are different. This may be due to model uncertainty, but may also hold meaningful geo-  
 21 physical signals. To explore this, we first computed a reference frame, in 10 Ma steps,  
 22 that adheres to a 'tectonic rule' that minimizes absolute total continent motion. We es-  
 23 timate the uncertainty by assigning a  $\pm 5$  Ma time window to the 10 Ma intervals and  
 24 find that the continent frame, or alternative frames based on an alternative 'rules', may  
 25 provide meaningful results for the last 350 Ma, but are unresolved before that time. With  
 26 this base frame, we predict hotspot trails, kimberlite and large igneous provinces erup-  
 27 tion sites, net lithosphere rotation, trench kinematics, and true polar wander, which are  
 28 all mostly within plausible ranges. We introduce this coupled frame as a Solid Earth In-  
 29 tegrated Reference Frame (SEIRF) that may be used (1) to aid interpretation of anoma-  
 30 lous geodynamic behavior; (2) to obtain novel constraints on mantle convection - the SEIRF  
 31 allows studying 'mantle kinematics' in a plate tectonic reference frame and (3) may serve  
 32 to train 3D numerical models of solid Earth dynamics.

## 33 Plain Language Summary

34 We observe the expressions of solid Earth dynamics at the Earth's surface in the  
 35 form of hotspot trails, trench kinematics, plate velocity, net lithosphere rotation, true  
 36 polar wander, and kimberlite and large igneous province eruptions. We may compute  
 37 these parameters given the absolute motion of plates relative to the mantle, but find-  
 38 ing true absolute plate motion, as well as true horizontal motion of the mantle remains  
 39 a challenge. Here, we approximate absolute plate motion relative to the mantle by as-  
 40 suming minimal continent velocity. The resulting mantle reference frame holds a pre-  
 41 diction for all expressions of plate-mantle interaction, which we dub the Solid Earth In-  
 42 tegrated Reference Frame (SEIRF). We show that by coupling all parameters within one  
 43 frame, we learn about solid Earth dynamics even without knowing true absolute plate  
 44 motion. For instance, we may investigate anomalous behavior in one parameter and see  
 45 if the anomaly fits with other parameters or exists in isolation. Moreover, with the SEIRF,  
 46 we may investigate relative motions between mantle sources of e.g. hotspots and kim-  
 47 berlites, which are independent of the absolute plate model. The SEIRF allows train-  
 48 ing of numerical models of solid Earth dynamics with all independent observations of  
 49 mantle behavior.

## 50 1 Introduction

51 The clearest expression of Earth's unique mode of mantle convection is plate tec-  
 52 tonics. Since the development of the theory of plate tectonics (McKenzie, 1969), plate  
 53 reconstructions have been used as basis to decipher the relative motions within the man-  
 54 tle, and between plates and the mantle, for instance using hotspot trails (e.g. Burke and  
 55 Wilson (1976)). This led to the development of 'mantle reference frames' that describe  
 56 the 'absolute' movement of tectonic plates relative to the mantle (e.g. Cox and Hart (1991))  
 57 Such frames (e.g. Duncan (1981); Müller et al. (1993); Duncan and Richards (1991); Le Pi-  
 58 chon et al. (2019); Torsvik, Burke, et al. (2010); Torsvik et al. (2006); Burke and Torsvik  
 59 (2004)) implicitly take as null hypothesis that active horizontal flow in the ambient man-  
 60 tle is negligible. Such reference frames are then used as basis to interrogate the null-hypothesis,  
 61 for instance, by analyzing how mantle flow may move hotspots relative to each other (Dobrovine  
 62 et al., 2012), how slabs may sink through the mantle (van der Meer et al., 2010), how

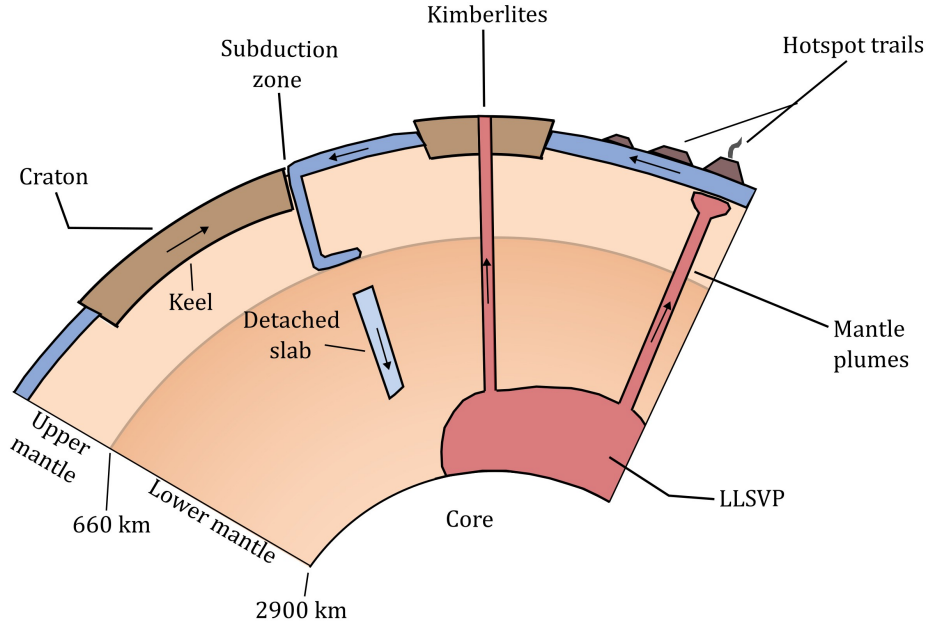


**Figure 1.** Schematic cross section of the mantle showing selected plate-mantle interactions. The black arrows indicate motion. LLSVP: Large Low Shear Velocity Province.

63 changes in Earth’s moment of inertia rotate the solid Earth relative to the spin axis (e.g.  
 64 (Steinberger & Torsvik, 2010)), or how rheological differences in the upper mantle may  
 65 lead to net lithosphere rotation (Conrad & Behn, 2010; Gérard et al., 2012). These and  
 66 many other processes within the mantle, or between mantle and lithosphere, are under-  
 67 pinned by independent geological and geophysical observations that led to many differ-  
 68 ent mantle reference frames. What is encouraging is that all frames predict similar be-  
 69 havior in terms of rates of absolute plate motions or subduction zone behavior, despite  
 70 being noticeably different (Becker et al., 2015; Torsvik et al., 2008; Williams et al., 2015;  
 71 Müller et al., 2022).

72 On the one hand, the differences between mantle reference frames may represent  
 73 uncertainties and noise. Under that assumption Tetley et al. (2019) recently introduced  
 74 a Tectonic Rules Model (TRM) that aimed to average differences. The TRM is a math-  
 75 ematical method that considers the observed kinematic surface expression of different  
 76 plate-mantle interactions (“tectonic rules”) and assigns each an (arbitrary) weighting to  
 77 compute an average (‘optimal’) absolute plate motion frame. On the other hand, the dif-  
 78 ferences may hold a meaningful geophysical signal that provides a unique way to con-  
 79 strain how, where, and when motions in the mantle occurred. In that case, the differ-  
 80 ent mantle reference frames should not be averaged, but the differences between should  
 81 be quantified and studied. Here, we use the TRMs ability to build mantle reference frames  
 82 from plate kinematic observations to explore that alternative possibility.

83 In this paper, we first calculate a mantle reference frame using one selected plate-  
 84 mantle interaction as a base model. To this end, we choose one of the ‘rules’ of the TRM  
 85 of Tetley et al. (2019), namely minimizing absolute continental plate motions, under the  
 86 null hypothesis that ambient horizontal upper mantle flow is negligible. We then esti-  
 87 mate uncertainty in this TRM frame, evaluating the effect of errors and uncertainties  
 88 in the plate circuit propagating back in time. Next, we compute the difference with other  
 89 observables of plate-mantle interaction and mantle convection (Figure 1). These include  
 90 trench migration, net lithosphere rotation, hotspot motion, eruption locations of large

igneous provinces and kimberlites, and true polar wander. This way, we aim to provide a next step towards creating an internally coherent, integrated set of kinematic constraints that include relative plate motions and relative mantle motions as constraint on solid Earth dynamics. Finally, we will discuss how these coupled properties aid in analyzing geological observations that may challenge the current status quo, how it may constrain mantle kinematics, and how it may contribute to training the next generation of 3D geodynamic numerical models.

## 2 Approach

### 2.1 Base model: continent frame

We use the TRM to optimize fit to one kinematic expression of plate-mantle interaction and determine misfit with other kinematic parameters. The original TRM (Tetley et al., 2019) included three "tectonic rules": minimizing hotspot misfit, minimizing absolute trench migration, and limiting net lithospheric rotation to a chosen maximum value, and was expanded to four "tectonic rules" with minimizing continent velocity in (Müller et al., 2022). These were then fitted simultaneously by weighting each model equally. Following Müller et al. (2022), we use the relative plate model of Merdith et al. (2021) as basis.

For practical reasons, we chose a 'continent frame' as base frame that can be computed with only a relative plate model as input. The continent frame assumes that plates that carry continents have deep keels into the upper mantle, which anchor the plate to the ambient mantle and resist absolute continent motion to minimize friction (Forsyth & Uyeda, 1975; Zahirovic et al., 2015). Motions of continents, which are tectonic features that may remain stable for hundreds of millions of years, are the best-constrained features in plate tectonic reconstructions. To build the continent frame, we construct a TRM that minimizes mean global velocity of continents. The TRM generates a  $1^\circ$  grid covering the Earth's surface and for each grid point determines the velocity vector. If a grid point exists within the continental polygons defined by Merdith et al. (2021), the velocity magnitude is included in the mean velocity. This method ensures the velocity of plates is weighted according to the area of continental crust they contain in the computation of the mean global continent velocity. The resulting mean velocity is minimized in a chosen, fixed time interval (here 10 Ma, in contrast to 5 Ma in Müller et al. (2022)). We slightly deviate from the TRM of Müller et al. (2022) by using the mean instead of the median global continental plate velocity. In absence of the other tectonic rules, using the median causes the TRM to keep any continental block exceeding 50% of all continental surface area fixed to obtain a zero median. Using the mean global continental plate velocity eliminates this artefact.

Evidently, any relative plate motion model that underpins the computation of a continent frame contains uncertainties and errors. Uncertainties in the positions of continents in plate models at a given reconstruction time stem for a large part from age uncertainties in the underlying data, such as in the dating of marine magnetic anomalies or the initiation and cessation of rifts and subduction zones. To evaluate possible effects of such age errors, we ran the TRM for the base frame ca. 180 times, each iteration drawing a new age range where each timestep is randomly selected from a  $10 \pm 5$  Ma window. For example, rather than a sequence of ages such as 10, 20, and 30 Ma, a random draw may produce a sequence such as 7, 19, and 32 Ma. The optimal pole reconstructing Africa relative to the mantle for each time window is collected per iteration and we calculate an uncertainty ellipse encompassing 95% of the poles using the Kent distribution (Kent, 1982).

139

## 2.2 Coupled properties

140

141

142

143

144

145

146

147

Next, we use the base model and the associated uncertainty to calculate (mis)fits to other plate-mantle interactions, as well as to the Earth’s magnetic field. These include (1) trench kinematics, (2) hotspots; (3) net lithosphere rotation; (4) kimberlite and large igneous province eruption sites relative to seismologically imaged deep-mantle structure; and (5) a paleomagnetic reference frame. Misfits with the base model may then result from (a) errors in the relative plate circuit, underestimation of base model uncertainty, or an invalid assumption underlying the base model, or (b) a meaningful geophysical signal of mantle dynamics.

148

### 2.2.1 Trench kinematics

149

150

151

152

153

154

155

156

157

158

159

160

161

162

163

164

165

166

167

168

169

170

171

172

173

174

175

176

177

178

179

180

181

182

183

184

An alternative mantle reference frame that seeks to minimize friction of tectonic plates with the underlying mantle is the ‘trench frame’, which assumes that the ambient mantle resists lateral motion of subducting slabs (Schellart et al., 2007, 2008; Spakman et al., 2018; Lallemand et al., 2005). In principle, a trench frame may therefore also be used as an alternative base model, as it builds on the same underlying assumption as the continent frame, and it was included in the TRM of Tetley et al. (2019); Müller et al. (2022). However, uncertainty in reconstructing subduction zones is much larger than uncertainty in reconstructing continents. Subduction zones are transient features and they may move relative to overriding plates, causing orogenic deformation and back-arc extension at plate margins, which needs to be included in the plate reconstruction (Müller et al., 2019; van Hinsbergen et al., 2011, 2020; van Hinsbergen & Schmid, 2012). This means that age uncertainty associated with the appearance and disappearance of a subduction zone, as well as with its position relative to stable plate interiors as a result of orogenic deformation comes on top of the uncertainty in rotations of the relative plate model, which makes it difficult to quantify. If the overriding plate is continental, remnants of ancient subduction zones are better preserved in the geological record and may be taken into account in plate reconstructions (e.g. van Hinsbergen et al. (2011)). Preservation of geological records of intra-oceanic subduction zones is poorer and although reconstruction is possible (Boschman et al., 2021; Stampfli & Borel, 2002; Clennett et al., 2020; Vaes et al., 2019; van de Lagemaat et al., 2024)), uncertainty is large. To illustrate, we computed a trench frame using the relative plate model of Merdith et al. (2021), but we note that even for Mesozoic and Cenozoic time, considerably different interpretations of intra-oceanic subduction are available. For instance, the Merdith et al. (2021) model contains few intra-oceanic subduction zones in the Pacific realm, whereas recent reconstructions offer solutions with tens of thousands of kilometers of intra-oceanic trenches (e.g. Vaes et al. (2019); Clennett et al. (2020); van de Lagemaat et al. (2024)). In addition, Merdith et al. (2021) contains a major intra-oceanic subduction zone within the eastern Neotethys ocean known as the conceptual ‘Trans-Tethyan arc’ that advances rapidly in the late Cretaceous Cenozoic (Martin et al., 2020), whereas alternative views offer solutions without such a trench (Advokaat & van Hinsbergen, 2024). It is beyond the scope of this paper to show how such differences may impact the predicted trench kinematics, or a minimum trench motion base frame, but they may strongly influence e.g. maximum rates of trench motion. In this paper, we take the reconstruction of Merdith et al. (2021) at face value to evaluate how robust reference frames based on minimizing friction may be. For this construction of the trench frame we use the global mean of absolute orthogonal trench migration, which is computed with

185

$$TM = \frac{\sum |V_i|}{T_n} \quad (1)$$

186

187

where  $|V_i|$  is the absolute magnitude of the trench-orthogonal velocity vector for each trench segment, and  $T_n$  is the number of trench segments.

188 In addition, trench kinematics are an intrinsic feature of any absolute plate model  
 189 and hold information on the dynamic interaction of individual slabs with the mantle they  
 190 subduct into. For present-day subduction zones, patterns of trench behavior are exten-  
 191 sively studied (Schellart et al., 2008; Lallemand et al., 2005; Williams et al., 2015; Fac-  
 192 cenna et al., 2007; Spakman et al., 2018; van de Lagemaat et al., 2018). Deviations of  
 193 trench kinematics in the continent frame from these patterns may thus invite scrutiny  
 194 of the plate reconstruction, or may signal atypical slab-mantle interaction. We therefore  
 195 compute the global mean and maximum trench retreat and advance rates, as well as the  
 196 mean and maximum trench-parallel slab dragging rates.

### 197 **2.2.2 Hotspot misfit**

198 Hotspot trails form by the progressive formation of volcanoes and are in their sim-  
 199 plest form the result of a plate moving over a fixed mantle source, generally thought to  
 200 represent a mantle plume (Wilson, 1963; Morgan, 1972; Duncan, 1981; Duncan & Richards,  
 201 1991; Müller et al., 1993). Reconstructions of hotspot trails show that hotspot sources  
 202 (plumes) may move slowly (<1 cm/yr) relative to each other (Steinberger, 2000; Tar-  
 203 duno & Cottrell, 1997; Doubrovine et al., 2012; O’Neill et al., 2005), although plume mi-  
 204 gration rate of up to 4 cm/yr has also been suggested (Tarduno et al., 2003), and plume-  
 205 lithosphere interaction may be remarkably long-lived (Torsvik et al., 2013; Rojas-Agramonte  
 206 et al., 2022). Any absolute plate motion model comes with a unique set of predicted hotspot  
 207 motions. We illustrate this by determining the predicted hotspot misfit and associated  
 208 required hotspot source motion for the base models using a selection of four long-lasting  
 209 hotspot trails: Hawaii and Louisville in the Pacific Ocean, Tristan in the Atlantic Ocean  
 210 and Reunion in the Indian Ocean. We computed the great-circle distance of each dated  
 211 point in these hotspot trails to the projected location in the base frames using the Haver-  
 212 sine equation

$$213 \quad d = 2r \sin^{-1} \left( \sqrt{\left( \frac{\phi_2 - \phi_1}{2} \right)^2 + \cos(\phi_1) \cos(\phi_2) \sin^2 \left( \frac{\lambda_2 - \lambda_1}{2} \right)} \right) \quad (2)$$

214 where  $d$  is the great-circle distance,  $r$  is the radius of the Earth,  $\phi_1$  and  $\phi_2$  are the  
 215 latitude of the two points in radians, and  $\lambda_1$  and  $\lambda_2$  are the longitude of the two points  
 216 in radians. In case of a misfit, we compute the predicted absolute motion of the hotspot  
 217 source. We interpolate the projected locations of the plume to 10 Ma intervals and com-  
 218 pute the misfit taking into account the uncertainty of the base model and the age un-  
 219 certainty of the dated hotspots and seamounts.

### 220 **2.2.3 Net lithospheric rotation**

221 Any absolute plate motion model comes with a unique value for net lithosphere ro-  
 222 tation. Net lithosphere rotation is calculated by summing all surface velocity vectors on  
 223 a grid and integrating the result over the surface of the Earth (Solomon et al., 1975; Torsvik,  
 224 Steinberger, et al., 2010). A non-zero value means that the lithosphere experiences a net  
 225 rotation relative to the underlying non-lithospheric mantle. Such a net rotation may re-  
 226 sult from artifacts, such as uncertainty or oversimplification in the plate reconstruction  
 227 (Torsvik, Steinberger, et al., 2010), but may also hold a meaningful geophysical signal.  
 228 A non-zero value of net rotation may result from lateral viscosity differences at the plate-  
 229 mantle interface that may cause variations in coupling of the lithosphere to the astheno-  
 230 sphere and thus variations in the resistance of plates to plate motion (Conrad & Behn,  
 231 2010; Becker, 2008; Atkins & Coltice, 2021; Gérard et al., 2012). Estimates of such cou-  
 232 pling for the present-day are inferred from seismic anisotropy (Becker, 2008). Values of  
 233 0.2-0.3°/Ma are deemed reasonable from geodynamic modelling (Conrad & Behn, 2010).  
 234 Higher numbers even up to 1.0°/Ma may signal anomalously low plate-mantle coupling,  
 235 e.g. due to reduced upper mantle viscosity and a spike in velocity of a particular plate

236 (Atkins & Coltice, 2021; G erault et al., 2012), but also invite scrutinizing the relative  
237 and absolute plate motion model (Torsvik, Steinberger, et al., 2010).

238 We calculate net rotation following the method described in Torsvik, Steinberger,  
239 et al. (2010) (Equation 3) using the optimal interval of 5 Ma as suggested in Atkins and  
240 Coltice (2021).

$$241 \quad \omega_{net} = 3/(8\pi r^4) \int v \times R dS = 3/(8\pi r^4) \sum_i \int (\omega_i \times R) \times R dS_i \quad (3)$$

242 where  $\omega_{net}$  is the NLR rate in degrees per million years,  $r$  is the radius of the Earth,  
243  $v$  is the velocity vector,  $R$  is the position vector,  $\omega_i$  is the angular velocity vector of plate  
244  $i$ ,  $\int ...dS$  indicates integration over the entire sphere,  $\sum_i$  indicates summation over all  
245 plates, and  $\int ...dS_i$  indicates integration over the area of plate  $i$ .

#### 246 **2.2.4 Kimberlite and LIPs versus LLSVP margins**

247 Burke and Torsvik (2004) found a correlation between the positions of modern deep-  
248 seated hotspots and the edges of the modern Large Low Shearwave Velocity Provinces  
249 (LLSVPs) at the core-mantle boundary as imaged in seismic tomography. In addition,  
250 they showed that when reconstructed in a hotspot mantle reference frame, also large ig-  
251 neous provinces (LIPs) appear to have formed above these edges (see also Torsvik et al.  
252 (2006); Burke et al. (2008)). These correlations were used to suggest that plumes are gen-  
253 erated along the edges of LLSVPs (the 'plume generation zones' of Burke et al. (2008)).  
254 Later, Torsvik, Burke, et al. (2010) found that also kimberlites, which are thought to re-  
255 sult from interactions of mantle plumes with cratonic mantle lithosphere, fit such a pat-  
256 tern, scattered in a zone of  $\sim 10^\circ$  around the margins of the modern LLSVPs. From this  
257 correlation it follows that prediction of the absolute eruption location of LIPs and kim-  
258 berlites invites scrutiny of their relation to the LLSVP margins through time. The pre-  
259 dicted eruption locations are directly coupled to the mantle reference frame and may form  
260 another constraint on a successful mantle model. For instance, if the eruption locations  
261 would systematically shift, this could indicate either absolute motion of the LLSVP mar-  
262 gins (as suggested by e.g. Bodur and Flament (2023)), or horizontal motions in the plume  
263 conduit (analogous to hotspot drift, e.g. Steinberger (2000)), or errors in the mantle re-  
264 ference frame or plate reconstruction. Therefore, we include the predicted eruptions lo-  
265 cations of LIPs and kimberlites into the SEIRF.

266 To this end, we used the LIP database of Burke and Torsvik (2004) and the kim-  
267 berlite database of Torsvik, Burke, et al. (2010), for the last 350 Ma. Note that Torsvik,  
268 Burke, et al. (2010) identified a cluster of outlying kimberlites in North America that  
269 did not erupt above the edges of the LLSVPs. We have omitted these data, so that the  
270 pattern of kimberlite eruption locations predicted by our base models may be compared  
271 to the pattern predicted by Torsvik, Burke, et al. (2010) based on their absolute refer-  
272 ence frames (based on the hybrid reference frame of Torsvik et al. (2008)).

#### 273 **2.2.5 True polar wander**

274 True Polar Wander (TPW) is the rotation of the solid Earth relative to the spin  
275 axis that results from changes in the moment of inertia (Goldreich & Toomre, 1969). Earth's  
276 moment of inertia may change due to motions of density anomalies through the man-  
277 tle, particularly subducting slabs (Steinberger & Torsvik, 2010). LLSVPs, which are cen-  
278 tered around the equator (Garnero, 2000) are thought to have a stabilizing effect on TPW  
279 (Steinberger & Torsvik, 2010). Moreover, the effect of subducting slabs on TPW is op-  
280 posite in the upper and lower mantle, such that the TPW oscillates and the net effect  
281 is zero (Steinberger & Torsvik, 2010; Steinberger et al., 2017). TPW is straightforwardly  
282 determined from the angular difference between a mantle reference frame and a paleo-

283 magnetic reference frame and has previously been computed using hotspot frames for  
 284 the time period for which hotspot data is available (e.g. Livermore et al. (1984); Besse  
 285 and Courtillot (2002); Doubrovine et al. (2012)). TPW computation for older times re-  
 286 lies on determining the common rotation of a plate circuit within a paleomagnetic frame  
 287 (Steinberger & Torsvik, 2008). Recent computations of TPW thereby assumed that TPW  
 288 in the past occurred around the same axis that corresponds to the modern moment of  
 289 inertia (0, 11° E), which is in the center of the LLSVP (Torsvik et al., 2014). Importantly,  
 290 this requires assumptions on the absolute paleolongitude of the plate circuit which is pa-  
 291 leomagnetically unconstrained (Torsvik et al., 2014). Moreover, TPW as recent as the  
 292 Cenozoic occurred along an axis that was almost orthogonal to 0, 11 ° E (Doubrovine  
 293 et al., 2012) (Vaes & van Hinsbergen, 2024). Strong deviations from previously computed  
 294 TPW values thus either require changes in the absolute paleolongitude of the plate cir-  
 295 cuit through time, or variation of the axis of TPW, which are intrinsically related to vari-  
 296 ations in Earth’s moment of inertia and the stabilizing role of the LLSVPs therein. This  
 297 forms an important potential source of information of solid Earth dynamics (Vaes & van  
 298 Hinsbergen, 2024). Therefore, we compute a prediction of TPW that follows from our  
 299 base frame by computing a TPW path by placing the global APWP of Vaes et al. (2023)  
 300 in our base mantle frame.

### 301 **3 Results**

#### 302 **3.1 Base frame: predicted motion path of Africa and uncertainty esti-** 303 **mates**

304 We used the reconstruction of Merdith et al. (2021) that provides a plate model  
 305 back to 1 Ga, to compute a continent frame (Table 1), and for comparison a trench frame,  
 306 in 10 Ma steps for the entire duration of the model. We then estimated the uncertainty  
 307 as outlined in the previous section, and determined how far back in time the absolute  
 308 plate motion in 10 Ma steps tends to exceed the uncertainty. We show the resulting ab-  
 309 solute plate motion paths in coordinates of Africa, for a location in the center of the African  
 310 continent (2°S, 16°E) (Figures 2a and 2b).

311 The trajectories of the two motion paths are at first order similar. Back to 120 Ma,  
 312 the continent frame computed migration of the African plate in a general NE direction.  
 313 While Pangea and further back Gondwana are unified, from ca. 570 Ma to 120 Ma, Africa  
 314 is kept fixed in place. In the period before the formation of Gondwana, between 570-620  
 315 Ma, the African plate is moved to the SW. This is preceded by a S-N loop between 620-  
 316 860 Ma following the break-up of Rodinia at ca. 860 Ma. From 1000-860 Ma, the cen-  
 317 tral African craton as part of Rodinia is once again kept fixed. The trench frame does  
 318 move Pangea in a E-W loop between ~120-400 Ma. The general W direction is maintained  
 319 while the African plate is part of Gondwana, with three N-S oscillations in the path. The  
 320 absolute movement of the African plate in the trench frame before the formation of Gond-  
 321 wana is roughly similar, although Rodinia is not kept as much in place.



**Table 1.** Total reconstruction poles of the absolute motion of the African plate in the Continent frame.

Time (Ma)	Latitude	Longitude	Angle
10	20.15	-26.68	-1.21
20	19.21	-23.06	-2.35
30	26.90	-21.40	-4.45
40	-29.63	158.45	7.06
50	-31.77	157.41	9.43
60	-32.56	154.42	10.66
70	-33.06	155.04	12.14
80	-34.39	156.94	15.66
90	35.29	-20.94	-20.16
100	35.40	-20.82	-25.56
110	34.92	-19.71	-31.16
120	33.50	-18.01	-37.14
130	32.36	-16.88	-39.59
140	31.24	-16.82	-41.29
150	30.65	-16.97	-42.16
160	29.67	-16.48	-43.31
170	28.79	-15.58	-44.75
180	28.51	-14.79	-45.31
190	28.42	-14.07	-45.67
200	28.34	-13.37	-46.00
210	28.32	-13.34	-46.02
220	28.32	-13.34	-46.02
230	28.32	-13.34	-46.02
240	28.32	-13.34	-46.02
250	28.32	-13.34	-46.02
260	28.32	-13.34	-46.02
270	28.32	-13.34	-46.02
280	-28.32	166.66	46.02
290	-28.32	166.66	46.02
300	-28.32	166.66	46.02
310	-28.32	166.66	46.02
320	-28.32	166.66	46.02
330	-28.32	166.66	46.02
340	-28.32	166.66	46.02
350	-28.32	166.66	46.02

### Motion paths of Africa since 1 Ga

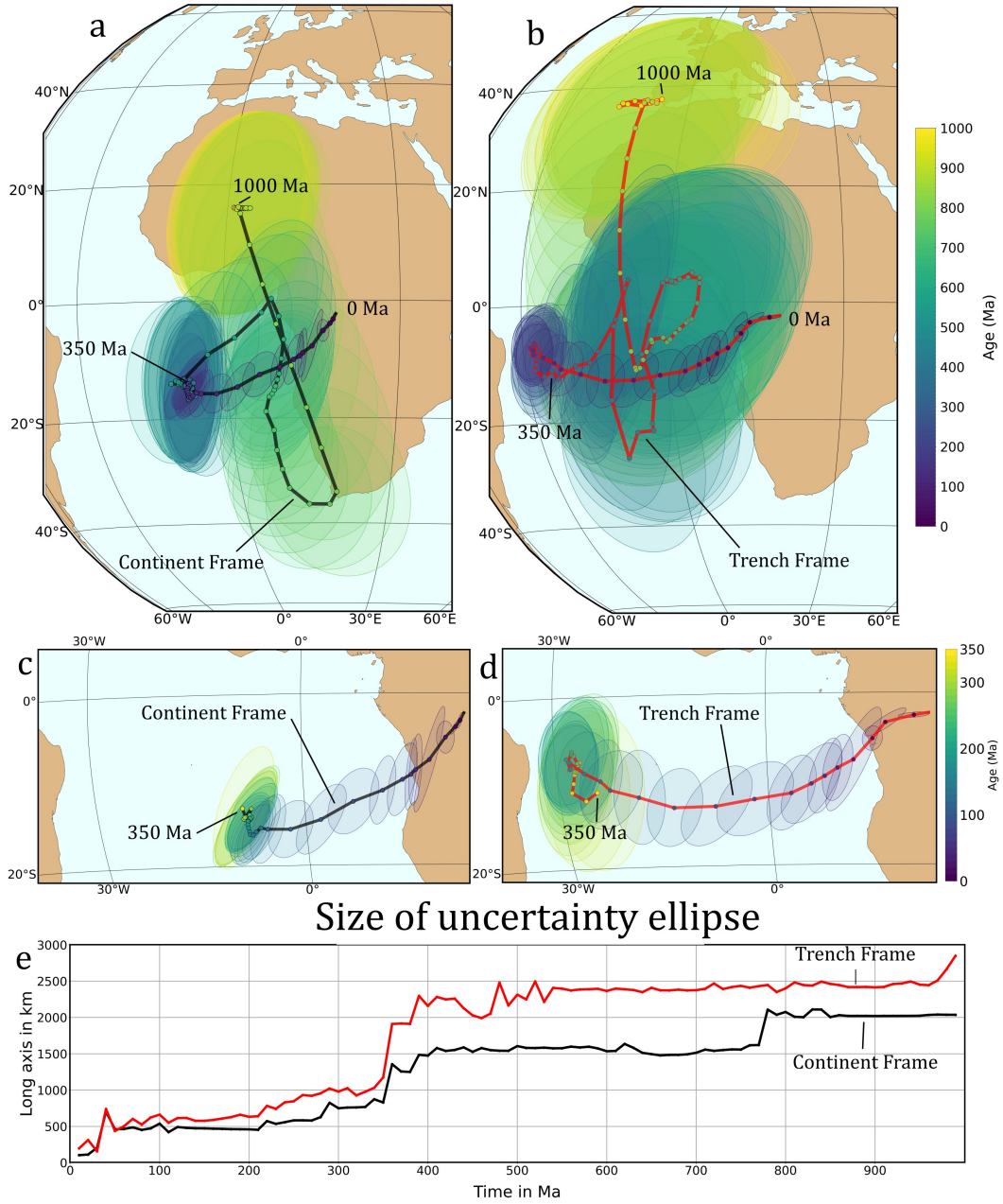


**Figure 2.** Motion paths from 1000-0 Ma of an arbitrary point in Central Africa in the continent (a) and trench (b) frames. The motion path is computed in 10 Ma time intervals with a  $\pm 5$  Ma window that results in an uncertainty ellipse encompassing  $2\sigma$  of all points. Subfigures (c) and (d) show the motion paths of Africa since 350 Ma for the continent and trench frame respectively. (e) The length of the long axis of the uncertainty ellipse over time for the continent frame (black) and trench frame (red).

322 The uncertainty estimates that follow from our 180 iterations varying the age win-  
 323 dows increases throughout time for both the continent frame and the trench frame (Fig-  
 324 ure 2e). The length of the long axis of the uncertainty ellipse in the continent frame rises

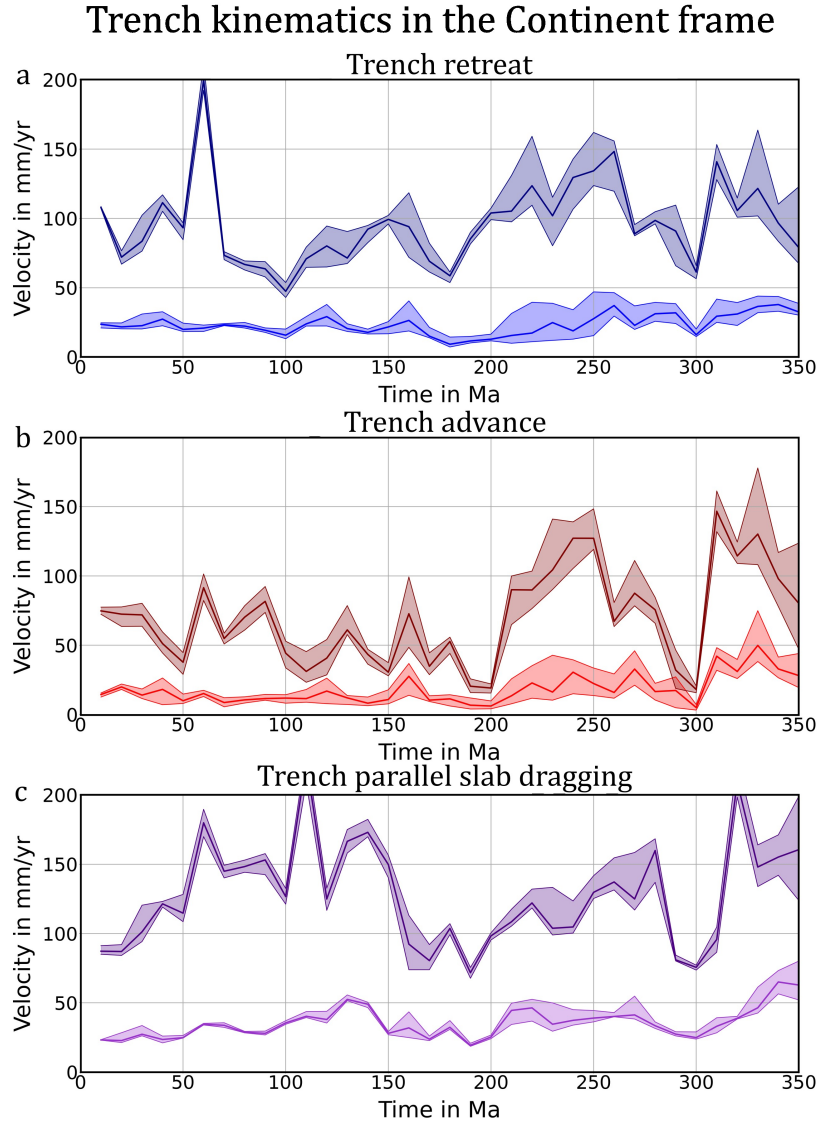


**Figure 3.** Trench kinematics as computed in the continent frame. (a) Orthogonal trench retreat, (b) orthogonal trench advance, (c) parallel slab dragging. The lighter shade represents the global mean value and the darker shade the maximum value computed for one trench segment. The schematic drawings on the right show how trench retreat is computed as the absolute orthogonal motion of the trench towards the subducting plate, how trench advance is computed as the absolute orthogonal motion of the trench towards the overriding plate, and how parallel slab dragging is computed as the absolute parallel motion of the subducting plate along the trench.

325 sharply back in time at 350 Ma and  $\sim 780$  Ma. These moments coincide with the formation of the supercontinents Pangea and Rodinia, in which major continents move in unison. The time periods before these supercontinents are associated with more complex modeled continent motions that are less well constrained and motion changes are more abrupt. The long axis of the uncertainty ellipse in the trench frame increases more than the continent frame at 350 Ma. Prior to 350 Ma, uncertainty ellipses in most cases encompass the magnitude of absolute plate motion when calculated in 10 Ma intervals. Ab-

326  
327  
328  
329  
330  
331

332 solute plate motions estimated with the TRM approach prior to 350 Ma in 10 Ma in-  
 333 tervals as used by Tetley et al. (2019) and in this paper, and especially in 5 Ma in-  
 334 tervals as in Müller et al. (2022), are thus unconstrained. In the following sections, we there-  
 335 fore focus on the time window of 350-0 Ma (Figures 2c and d).

## 336 **3.2 Coupled properties**

337 We now explore how the coupled properties behave in the base frame, for which  
 338 we chose the continent frame.

### 339 **3.2.1 Trench kinematics**

340 Our base frame predicts values for the mean orthogonal trench retreat and trench  
 341 advance rates that are on the order of 2-5 cm/yr for times after  $\sim$ 200 Ma (Figure 3a and  
 342 b respectively). This is within the range computed for the present day (Schellart et al.,  
 343 2008). Trench-parallel slab dragging rates are in the same range (Figure 3c), which com-  
 344 pares well with reconstructed examples (van de Lagemaat et al., 2018; Parsons et al., 2021),  
 345 although no global means have so far been computed. The computed values for the max-  
 346 imum rates are high and contain sharp spikes, which may indicate errors in the plate model  
 347 or narrow trenches obeying motions of large surrounding plates. Prior to 200 Ma, the  
 348 maximum value for trench advance rises to 10-15 cm/yr, which is caused by rapid trench  
 349 migration of reconstructed narrow trenches in the Tethys Oceans in the relative plate  
 350 model of Merdith et al. (2021).

### 351 **3.2.2 Hotspot trails**

352 We may now use our base model to predict hotspot trails assuming hotspot fixity.  
 353 The four hotspot trails that we selected in the Pacific (Hawai'i-Emperor, Louisville), At-  
 354 lantic (Tristan), and Indian oceans (Reunion) overall fit the predicted trails, although  
 355 deviations are obvious (Figure 4). We infer from this that the base frame may represent  
 356 a reasonable starting point towards an absolute plate motion frame. The description be-  
 357 low of apparent hotspot source motion should thus not be taken as an interpretation of  
 358 geological history, but as an illustration of how constraints from hotspots may be used  
 359 in a SEIRF.

360 The Hawai'i-Emperor hotspot trail, which in previous moving hotspot models and  
 361 in numerical experiments is often hypothesized to be among the fastest moving ones (Dobrovine  
 362 et al., 2012; Hassan et al., 2016), as well as from paleomagnetic data (Tarduno et al., 2003).  
 363 Interestingly, our base frame predicts the Hawai'i-Emperor hotspot trail, including its  
 364 marked kink around 45-50 Ma, surprisingly well assuming hotspot fixity (Figure 4a). If  
 365 our base model would be correct, it would predict some hotspot motion, because the pre-  
 366 dicted trail lags slightly behind the observed trail, i.e. our Pacific plate moves in the right  
 367 direction but either the plate is too slow or the hotspot source moved slowly. Some south-  
 368 ward absolute hotspot source motion is barely larger than the uncertainty ellipses (Fig-  
 369 ure 4e). Also for the Louisville hotspot, the continent frame predicts the real trail re-  
 370 markably well (Figure 4b) and the hotspot source would within error be nearly fixed rel-  
 371 ative to the mantle (Figure 4f).

372 The base frame predicts the last 60 Ma of the Reunion trail, located on the African/Somalian  
 373 plate well (Figure 4c), with no more than about  $2^\circ$  of hotspot source migration since that  
 374 time (Figure 4g). Finally, for the Tristan hotspot, the base frame predicts the hotspot  
 375 trail well for the last 60 Ma, whereas between 130-60 Ma the predicted trail and refer-  
 376 ence trail deviate increasingly back in time (Figure 4d). Accordingly, the predicted plume  
 377 migration is practically zero for 0-60 Ma, while between 130-60 Ma, the hotspot source  
 378 is predicted to migrate ca.  $13^\circ$  in a fairly continuous motion to the southeast (Figure  
 379 4h).

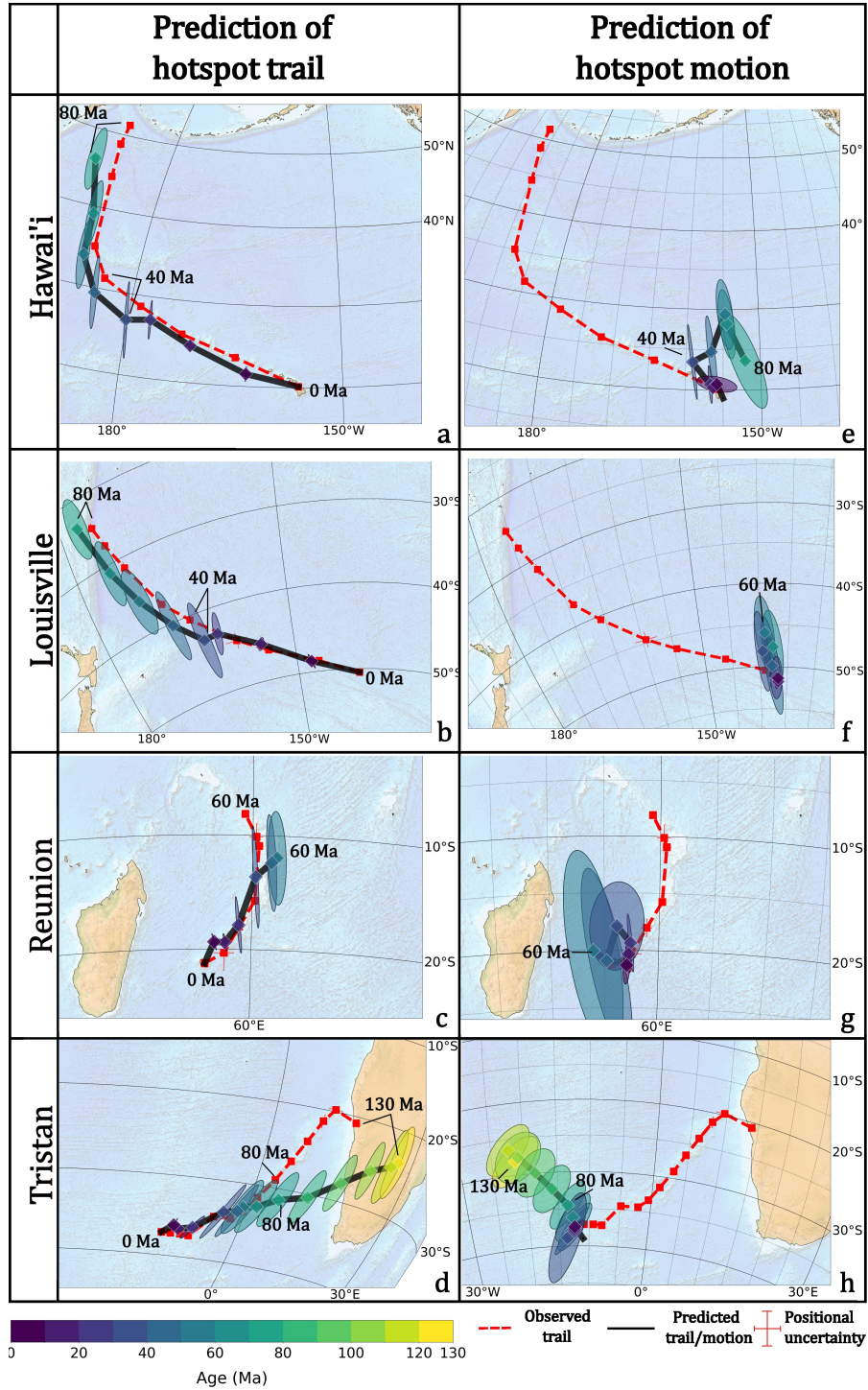


**Figure 4.** The prediction of selected hotspot trails in the continent frame. The black line represents the predicted trail or the predicted hotspot source motion in the continent frame and the black dashed path represents the observed trail. The predicted trails and source motion are calculated to 10 Ma time intervals. Each point includes an uncertainty ellipse from the age uncertainty estimate, which are colored according to time. The reference trails are interpolated to 10 Ma intervals and include the positional uncertainty arising from the age uncertainty of the volcanic islands and seamounts, which is marked with red error bars.

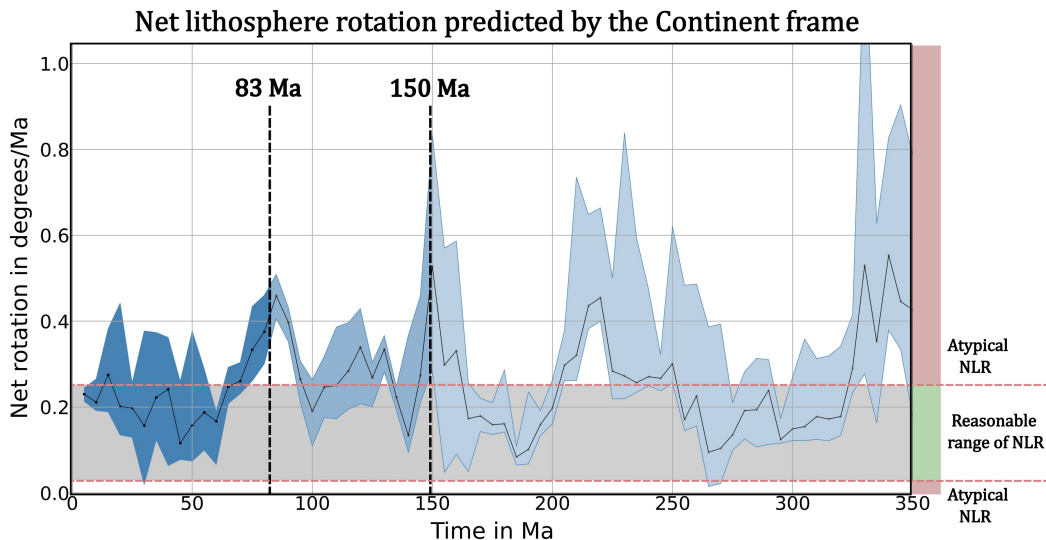


**Figure 5.** Predicted net lithospheric rotation in the base frame, correlated over 5 Ma time intervals. The red dashed line shows the maximum expected value for net rotation from geodynamic modelling (Becker, 2008; Conrad & Behn, 2010). The time period prior to 83 and 150 Ma is marked and faded out, to indicate the diminished robustness of the net rotation computation due to losing the plate tectonic connections to the plates in the Pacific realm.

380

### 3.2.3 Net lithosphere rotation

381

382

383

384

385

386

387

388

389

390

391

392

393

394

395

396

For much of the last 350 Ma, the computed net rotation values lie within the 0-0.3°/Ma range that is within the range for the present day (Becker, 2008; Conrad & Behn, 2010), although there are notable peaks (Figure 5). A period of higher net rotation occurs between 75-95 Ma, peaking at 0.5°/Ma at 85 Ma. These values stem from the reconstruction of very high velocity (>20 cm/yr) of a fast-moving plate in the NW paleo-Pacific realm (Izanagi plate) in this time (Merdith et al., 2021; Lin et al., 2022). If such peaks are the result of lateral viscosity contrasts in the upper mantle, they hold interesting geodynamic information. However, they may also result from errors in the plate reconstruction, whereby oceanic plates - having large surface areas and high velocities - have a large influence. Prior to 83 Ma, the connection of the Pacific plates to the Indo-Atlantic plates through Antarctica is lost, adding considerable uncertainty (Dobrovine & Tarduno, 2008). Prior to 150 Ma, hotspot control on Pacific plate motion is absent (Torsvik & Cocks, 2019) and interpretation of oceanic plates and intra-oceanic subduction zones in the Panthalassa Ocean differs strongly between authors (Merdith et al., 2021; Boschman et al., 2021; van de Lagemaat et al., 2023; Lin et al., 2022). It is therefore challenging to straightforwardly identify plate modelling artefacts from true net rotation before 83 Ma.

397

### 3.2.4 Kimberlite and LIPs reconstruction

398

399

400

401

402

403

404

Our base frame predicts the locations of kimberlites and LIPs at time of eruption relative to the edges of the present-day LLSVPs. Kimberlites and LIPs for the last 350 Ma cluster on the edges of LLSVPs (Figure 6). In addition, the predicted motions of the Indo-Atlantic hotspots occur more or less along the edges of the African LLSVP (Figure 6). What stands out is a notable eastward shift in kimberlite and LIP sources in the Atlantic realm during the Cretaceous, ~120-80 Ma. This shift would mean that kimberlite sources in southern Africa reconstructed above the outer edge of the modern African

## Reconstructed kimberlite, large igneous province, and hotspot eruption locations in the Continent frame

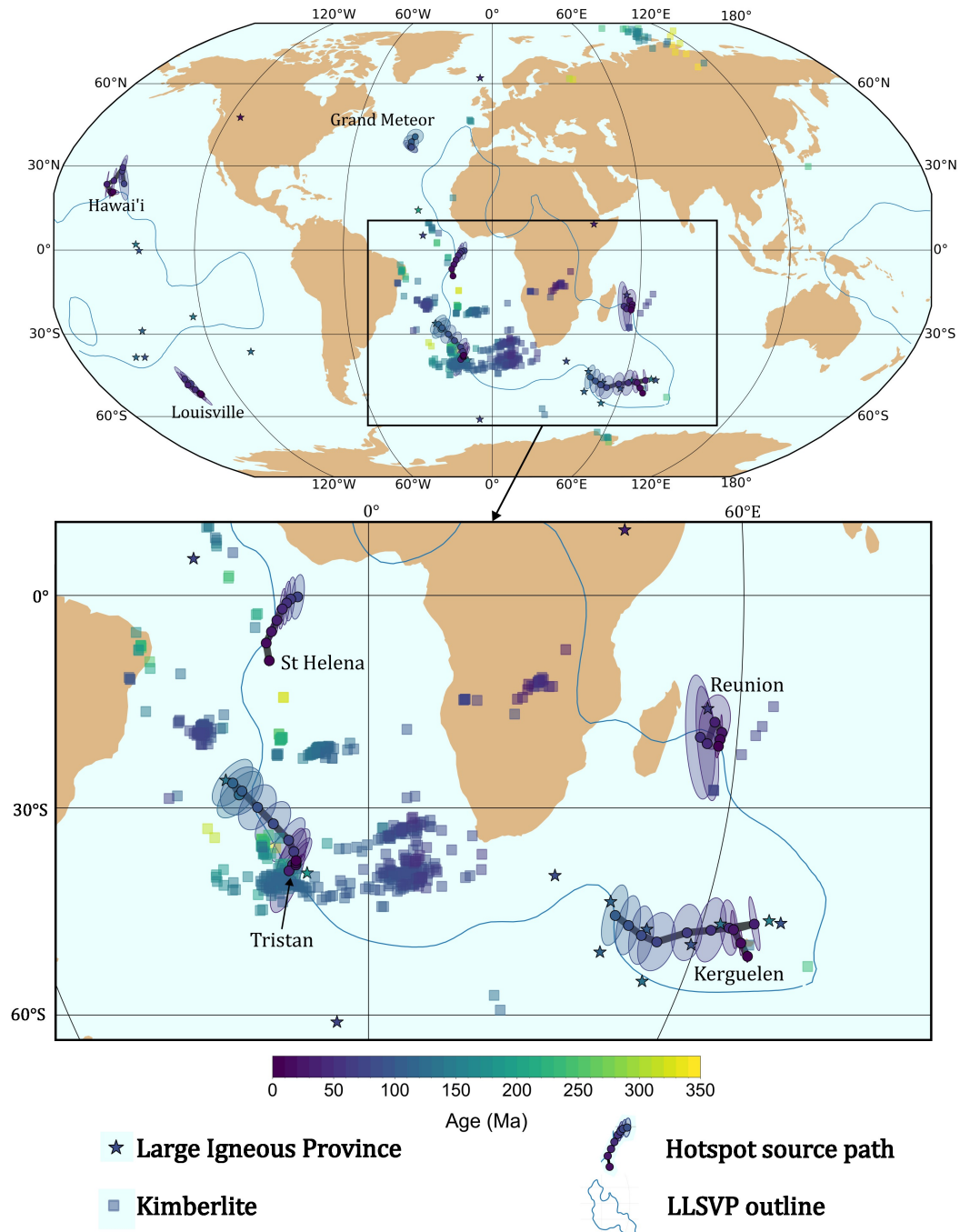


**Figure 6.** The reconstructed locations of kimberlite eruption sites (square), LIP eruption sites (star), and selected hotspot eruption sites in the continent frame. The LLSVP outline plotted is the 1% slow contour of the SMEAN tomographic model at 2800 km (Torsvik et al., 2014). LIP eruption sites and hotspot eruption sites are plotted with an uncertainty ellipse representing the age uncertainty in the base frame.

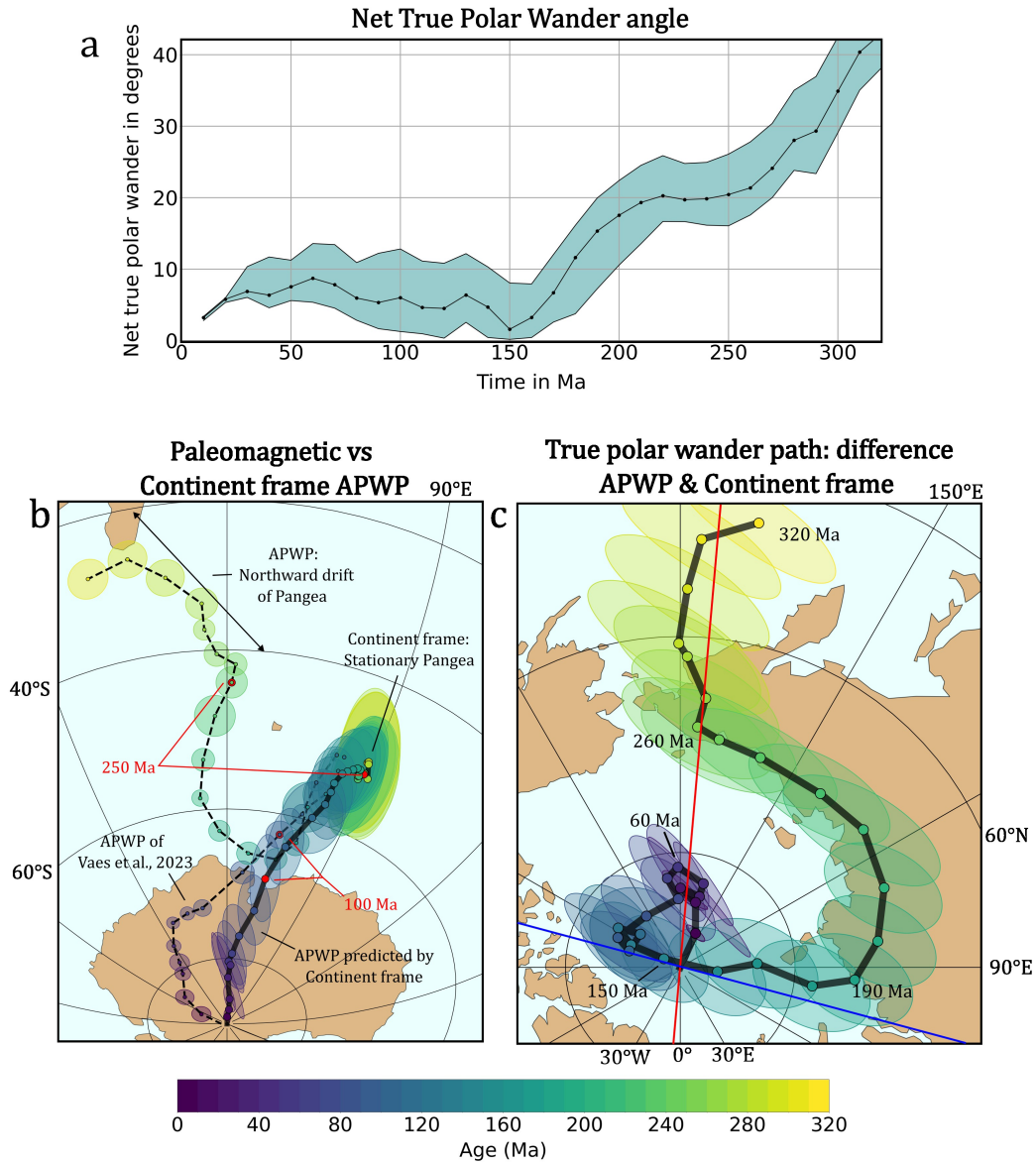


**Figure 7.** TPW predictions for the base frame. (a) Angular difference between the base frame and the paleomagnetic frame. (b) Paleomagnetic APWP (Vaes et al., 2023) (black dashed line) and synthetic APWP of the continent frame (black solid line) plotted on the South Pole. (c) True Polar Wander Path (TPWP) of the continent frame plotted on the North Pole. The axis around 0°/15°W is marked with a blue line and the axis around 0°/85°E is marked with a red line.

405 LLSVP from 320-120 Ma and shifted eastward until ~50 Ma, after which kimberlite vol-  
 406 canism stopped (Figure 6).

407 **3.2.5 True polar wander**

408 Finally, we computed a TPW frame for the last 320 Ma by placing the recent pa-  
 409 leomagnetic reference frame of Vaes et al. (2023) in our base frame. Our continent frame



410 predicts a net TPW rotation of  $\sim 9^\circ$  since 60 Ma (Figure 7a), consistent with estimates  
 411 based on hotspot reference frames (Dobrovine et al., 2012; Vaes & van Hinsbergen, 2024).  
 412 The TPW path suggests that cumulative TPW since 150 Ma is close to zero, as indicated  
 413 by the spin axis plotting close to the geographic pole (Figure 7c). Between 150 and 190  
 414 Ma, a large shift in the estimated position of the spin axis predicts a TPW rotation of  
 415  $\sim 20^\circ$  about an equatorial axis located close to  $0^\circ\text{E}$ . This is notably similar to previous es-  
 416 timates of TPW who indicated a  $\sim 20^\circ$  rotation during the Jurassic about an axis located  
 417 at  $0^\circ/11^\circ\text{E}$  (Torsvik et al., 2014) and  $0^\circ/15^\circ\text{W}$  (Vaes & van Hinsbergen, 2024)

418 Prior to  $\sim 200$  Ma, our continent frame minimizes the motion of Africa (i.e., Pangea)  
 419 relative to the mantle (Figure 7b). As a result, the TPW path becomes very similar to  
 420 the global APWP. The large swing observed in the global APWP during the Triassic,  
 421 as well as the  $\sim 20^\circ$  shift in the pole position between 250 and 320 Ma due to the north-  
 422 ward motion of Pangea, are also clearly visible in the TPW path. Consequently, the net  
 423 angle of TPW predicted by the base frame increases back into geological time and be-  
 424 comes as much as  $40^\circ$  at 320 Ma (Figure 7a). This is in sharp contrast with previous es-  
 425 timates of TPW by Torsvik et al. (2012, 2014), who reconstructed no significant TPW  
 426 between 250 and 320 Ma. The difference between the TPW prediction of our base frame  
 427 and the estimates of e.g., Torsvik et al. (2012, 2014) stems from the assumption that TPW  
 428 occurred around an axis located at  $0^\circ/11^\circ\text{E}$ . Instead, they interpreted the paleolatitu-  
 429 dinal component of the motion of Pangea, which would correspond to an axis orthog-  
 430 onal to  $0^\circ/11^\circ\text{E}$  (Figure 7c), as reflecting plate motion over the mantle. This implies that  
 431 Pangea underwent major northward plate motion between 320 and 250 Ma. On the other  
 432 hand, our base frame suggests that Pangea's northward drift was almost entirely a re-  
 433 sult of TPW. Although attributing all northward motion to TPW may be extreme, large  
 434 amplitude TPW during this interval, as previously proposed by Le Pichon et al. (2023);  
 435 Vaes and van Hinsbergen (2024) would have intriguing implications. Namely, it would  
 436 predict that the LLSVPs, whose modern center of mass lies close to the inferred TPW  
 437 axis at  $0^\circ/11^\circ\text{E}$  of Torsvik et al. (2014), moved relative to the equator during a major  
 438 phase of TPW (if they remained stationary in the mantle). We will return to the im-  
 439 plications of such predictions in the discussion.

## 440 4 Discussion

### 441 4.1 A Solid Earth Integrated Reference Frame with a Continent Frame 442 as basis

443 To use plate tectonic history to constrain the dynamic workings of the mantle re-  
 444 quires placing plate tectonic reconstructions in a mantle reference frame. A 'reference  
 445 frame' shows the motions of plates relative to a chosen fixed point, which introduces a  
 446 problem: the mantle must accommodate the sinking of slabs, the upwelling of mantle  
 447 below ridges, and the rise of mantle plumes and thus cannot be a fixed body of rock. In  
 448 fact, plate motions in a mantle 'reference frame' are used to estimate how the mantle  
 449 is moving. This is likely one of the reasons why different estimates of absolute plate mo-  
 450 tion, using hotspots, net lithosphere rotation, or true polar wander-corrected paleomag-  
 451 netic frames combined with trench-slab correlations, or kimberlite/LIP-LLSVP corre-  
 452 lations, do not yield identical results. All estimates of plate-mantle interaction are con-  
 453 nected to each other via the relative plate model and give some assumed 'base' mantle  
 454 reference frame, the motions of independent plate-mantle interactions, and rotation of  
 455 the solid Earth relative to the spin axis (true polar wander) is constrained. We dub this  
 456 a Solid Earth Integrated Reference Frame (SEIRF) (Figure 8), in which independent ob-  
 457 servations of plate-mantle interaction are tied together, sharing one key unknown: true  
 458 absolute plate motion.

459 Our base frame of minimum continental plate velocity is based on the common null  
 460 hypothesis in which horizontal motions in the mantle are insignificant. This is the same

461 null hypothesis that implicitly underlies classical fixed hotspot frames (e.g. Müller et al.  
 462 (1993)), namely that horizontal motions in the ambient mantle are negligible. This 'con-  
 463 tinent frame', previously used in combination with other approaches in the computation  
 464 of a TRM (Müller et al., 2022), but not computed as a separate mantle reference frame,  
 465 may thus approximate, but cannot represent true absolute plate motion. Moreover, it  
 466 is important to note that this continent frame, like all other reference frames, is unique  
 467 to a given relative plate motion model. Our version (Table 1) is thus specifically com-  
 468 puted for the relative plate motion model of Merdith et al. (2021), and would require re-  
 469 calculation for plate models with different underlying Euler rotations or continent con-  
 470 figurations.

471 The main advantage of the continent frame lies in the simple underlying null hy-  
 472 pothesis. It can be calculated for all times a relative plate model, versions of which have  
 473 been proposed for times as far back as 1.8 Ga (Cao et al., 2024). However, our estimates  
 474 of uncertainty, which only illustrate the effect a  $\pm 5$  Ma age uncertainty in the data that  
 475 underlie the relative plate reconstruction, reveal the challenges constraining absolute plate  
 476 motion in deep geological time (Figure 2e). For times between 350 Ma and 0 Ma, the  
 477 relative positions of most continents are well-constrained through ocean basin reconstruc-  
 478 tions, and connections of continents within Pangea, and uncertainty in the relative plate  
 479 model concerns mostly the reconstruction of oceanic plates, for which the continent frame  
 480 is immune. For times prior to 350 Ma, and especially back into the Precambrian, a  $\pm 5$   
 481 Ma age uncertainty is likely not conservative enough. Moreover, in absence of ocean basins  
 482 to reconstruct, major uncertainty in pre-Pangean plate motions arise (Buffan et al., 2023;  
 483 Seton et al., 2023), particularly in paleolongitude (e.g. Domeier and Torsvik (2019)), whose  
 484 effects should be added to the age uncertainty. With error bars already exceeding ab-  
 485 solute plate motions in the 10 Ma intervals we used, using just a  $\pm 5$  Ma uncertainty (Fig-  
 486 ure 2e), absolute motions in continent or trench frames, or combinations thereof in a TRM  
 487 (Müller et al., 2022) for times prior to 350 Ma must be considered unresolved.

488 On the other hand, our estimated uncertainty of the continent frame after 350 Ma  
 489 may be a reasonable approximation, and the 10 Ma steps used in absolute plate motion  
 490 exceed those uncertainties. The continent frame predicts an encouragingly good fit with  
 491 the Pacific hotspot trails, and provides reasonable numbers for net rotation, TPW, trench  
 492 kinematics, and hotspot drift rates, as well as LLSVP-kimberlite/LIP fits. We therefore  
 493 consider it a good starting point to interrogate geodynamics and absolute plate motions.

## 494 **4.2 Using coupled properties to investigate geodynamic signal and noise**

495 One application of the SEIRF is that it allows interrogating the geodynamic plau-  
 496 sibility of surprising spikes in the prediction of one of its kinematic components. Such  
 497 spikes may indicate an interesting geodynamic conundrum that would present an oppor-  
 498 tunity to challenge the state-of-the-art but should first invite scrutiny of the relative plate  
 499 model (see also Clennett et al. (2023)). From many candidates, we selected three exam-  
 500 ples to illustrate the use of independent properties coupled in the SEIRF. For instance,  
 501 the continent frame predicts very high trench migration rate for several narrow subduc-  
 502 tion zones in the Tethys Ocean during the Triassic. If true, then this may inform about  
 503 e.g. anomalously low viscosity in the mantle below the Tethys Ocean. However, given  
 504 the challenges to accurately reconstruct intra-oceanic subduction history in ocean basins  
 505 that have been lost to subduction (e.g. Vaes et al. (2019); Boschman et al. (2021)), this  
 506 case is for now better conservatively interpreted as reconstruction error, and investiga-  
 507 tion into the relative plate model is the better first step.

508 Another interesting signal arises from the spike in net lithosphere rotation in the  
 509 late Cretaceous caused by rapid motion of the Izanagi plate in the northwest paleo-Pacific  
 510 realm (Lin et al., 2022). This spike in net rotation (Figure 5), could for instance suggest  
 511 a weakened plate coupling to the asthenosphere facilitating rapid plate motion. An in-

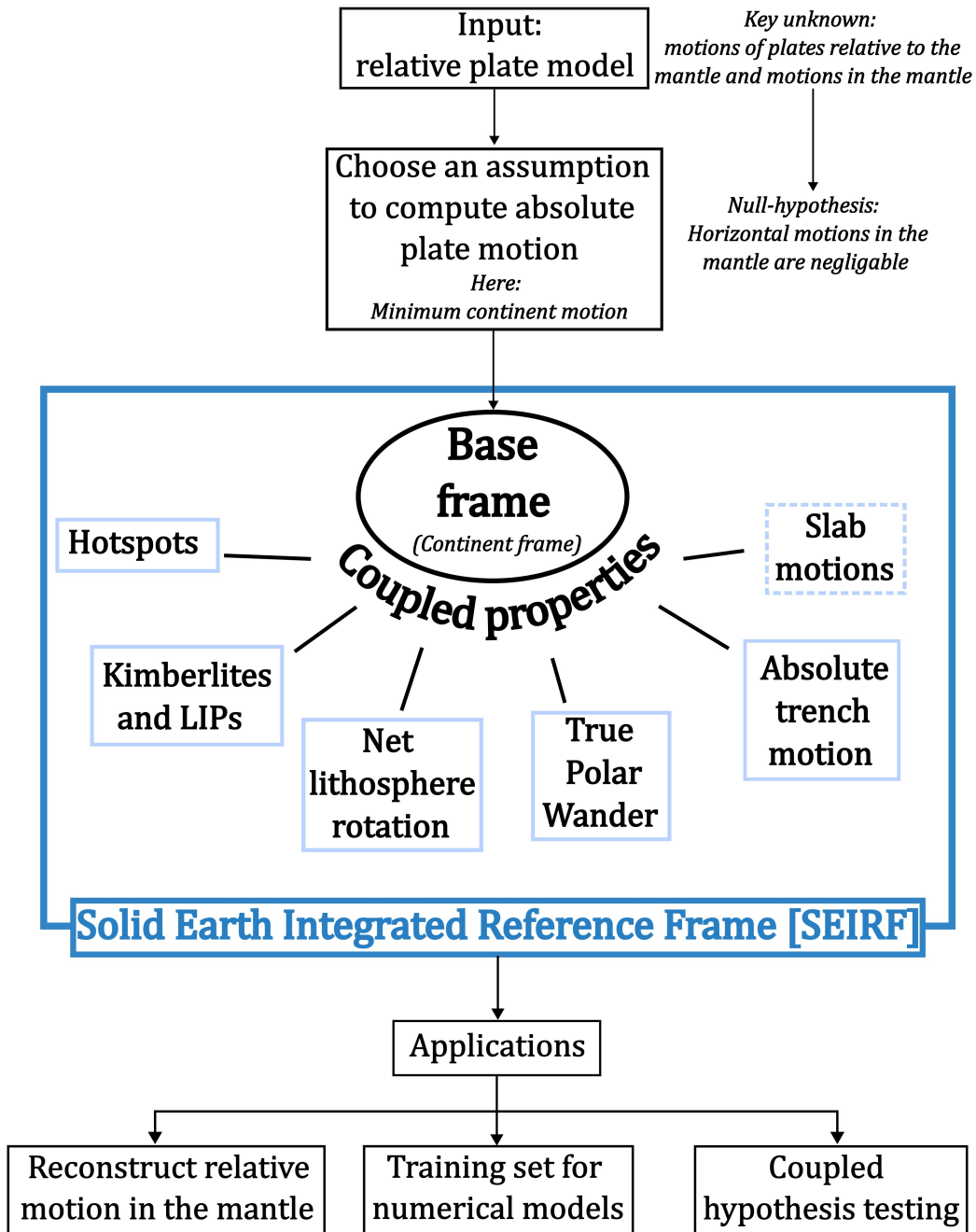


**Figure 8.** Schematic overview of the construction of the SEIRF and its components.

512 dependent evaluation of that implication could come from reconstructions of trench mi-  
 513 gration in the northwest paleo-Pacific realm. Orogenic belts on Kamchatka show evidence  
 514 for long-lived intra-oceanic subduction in late Cretaceous to Paleogene time (Konstantinovskaia,  
 515 2001). The plate model of Meredith et al. (2021) did not include this detailed reconstruc-  
 516 tion of intra-oceanic subduction. However, those that do (Domeier et al., 2017; Vaes et  
 517 al., 2019), constrained among others by independent paleomagnetic data, reveal rapid  
 518 paleolatitudinal motion of intra-oceanic arcs, and associated trenches must have had high,  
 519 long-lived trench retreat. Such rapid trench motions could form an independent argu-

ment for an anomalously weak mantle. Within context of the SEIRF, the regional plate reconstruction of e.g. Vaes et al. (2019) should be included into the global plate reconstruction, and the base frame and associated net rotation should be recalculated.

Finally, the phase of northward migration of Pangea in the late Permian to early Triassic that is observed in the paleomagnetic reference frame is absent from the continent frame. We computed this using the recent site-level based global apparent polar wander path of Vaes et al. (2023), but previous renditions based on traditional statistical procedures (Torsvik et al., 2012) showed the same pattern and would not significantly change this Pangean paleolatitudinal motion estimate. We find that within the continent frame, this migration is almost entirely attributed to TPW, with a magnitude as high as  $40^\circ$  or more (Figure 7a). Major TPW moving Pangea northward was postulated before (e.g. Le Pichon et al. (2021)), but the magnitude far exceeds previous estimates based on finding common rotations around the current center of mass of the LLSVPs (Torsvik et al., 2014). We may use the different observations in the SEIRF to search where possible solutions may lie. The continent frame does not identify Pangean latitudinal motion as plate tectonic behavior, because moving the supercontinent at such speeds would lead to major friction. It would require long-lived extensive trench-parallel slab dragging of the subduction zones on the N-S trending Pangean margins, which also induces friction and has no local geodynamic driver (Spakman et al., 2018). The plate reconstruction of Meredith et al. (2021) does not contain major subducting oceanic plates attached to the supercontinent that could readily explain such movement. The sources of kimberlites in Southern Africa in this time window are predicted by the continent frame to remain stable and aligned with the LLSVPs, fitting previously inferred patterns (Torsvik, Burke, et al., 2010) whereas reconstructing northward Pangean plate motion would require comparable migration of kimberlite sources. Moreover, as we already pointed out in section 3.2.5, the previous estimates of Pangean TPW essentially assumed an axis of TPW within the heart of Pangea (Torsvik et al., 2014). If that axis would instead have been located far west or east, as appears to be the case for much of the Cenozoic (Dobrovine et al., 2012; Vaes & van Hinsbergen, 2024), paleolatitudinal motion of Pangea due to TPW could have been underestimated. Those combined observations could invite re-investigation of a hitherto controversial interpretation of Pangean paleolatitudinal change.

However, the continent frame, and the argument of slab dragging resisted by the mantle, relies on the assumption of negligible horizontal ambient mantle flow. Should a northward mantle flow have existed below Pangea, our base frame, and the interpretation of trench kinematics, would change. The geodynamic likelihood of such an alternative could be tested in numerical experiments. Moreover, such high TPW must reflect major changes in the Earth’s moment of inertia, whose causes are typically best sought in the disturbing role in the subduction of slabs and the stabilizing role of LLSVPs (Steinberger & Torsvik, 2010). Interpreting a major syn-Pangea TPW phase thus invites investigating such causes of the change in Earth’s moment of inertia, introducing more independent datasets. These examples illustrate that the SEIRF provides a framework to analyze one hypothesis using independent, but coupled constraints.

### 4.3 Reconstructing relative motions in the mantle

Because the continent frame holds no assumptions on mantle structure, the SEIRF provides a means to determine relative motions in the mantle, even if the base mantle reference frame is incorrect. In part, relative motions between geological observations that are tied to the mantle are already evident in the relative plate model. The best example is the evidence for hotspot drift, which follows from relative motion between the Pacific and Indo-Atlantic hotspots (e.g. Steinberger (2000)). In the same manner, relative motions between hotspots and kimberlite eruption sites could be constrained. But when placed in a base mantle reference frame, also motions relative to presumed plume sources (e.g., the edges of LLSVPs (Burke & Torsvik, 2004)) may be investigated. For

572 instance, the continent frame suggests that the Pacific hotspots of Hawai'i and Louisville  
 573 are almost stationary and that most plume motions occur in the Indo-Atlantic domain.  
 574 Interestingly, the continent frame predicts motion of the Tristan, St Helena, and Ker-  
 575 guelen hotspot source (plume) along the LLSVP edge (Figure 6), which could be used  
 576 to investigate a deep-mantle flow effect. Meanwhile, the kimberlite sources migrated in  
 577 the direction of absolute plate motion, and more or less parallel to the southeastern mar-  
 578 gin of Africa, and could show the effect of the continental keel on a mantle plume. Such  
 579 hypotheses naturally depend on the absolute plate model and change therein may change  
 580 the hypotheses, but the relative motion between the Tristan hotspot source and the kim-  
 581 berlite source remains independent of the absolute plate model (similar to Rose et al.  
 582 (2022)).

583 Further information on the causes of plume motion may come from incorporation  
 584 of slabs imaged in the mantle (manifested as high seismic wave velocity anomalies) and  
 585 subduction-related orogens into the SEIRF. Such correlations have been made before,  
 586 and were used to determine slab sinking rates (van der Meer et al., 2010, 2018; Butter-  
 587 worth et al., 2014), as a semi-quantitative estimate of absolute plate motion (van der Meer  
 588 et al., 2010), and even to interpret intra-oceanic subduction zone reconstructions (Van der  
 589 Meer et al., 2012; Sigloch & Mihalynuk, 2013). By considering these slab-trench corre-  
 590 lations within the SEIRF, we may reconstruct whether slabs, during or after their de-  
 591 tachment, must have also moved horizontally relative to one another, and relative to plumes.  
 592 The absolute direction of the reconstructed motion remains dependent on the absolute  
 593 plate motion (opening possibilities to cross-correlate with e.g. seismic anisotropy (Wolf  
 594 & Long, 2023)), but the relative motion does not. However, currently the localization  
 595 of slab edges and midpoints remains qualitative and lacks detail (van der Meer et al.,  
 596 2018). We identify quantifying the location of slab edges in the mantle in an objective  
 597 manner as a key next step in correlating slabs to coordinates in the plate circuit.

#### 598 **4.4 SEIRF as training set to calibrate numerical models**

599 Finally, the coupled observables of plate-mantle interaction in the SEIRF hold the  
 600 potential for calibrating numerical mantle models. True 'absolute' plate motion is only  
 601 known in controlled numerical experiments that include both plate motion and mantle  
 602 flow, in which mantle flow influences the constraints on plate-mantle motion. Such an  
 603 integrated numerical-kinematic approach was underlying the development of 'moving hotspot  
 604 reference frames' (O'Neill et al., 2005; Torsvik et al., 2008; Doubrovine et al., 2012) in  
 605 which numerical models were driven by an 'absolute' plate motion model first assum-  
 606 ing hotspot fixity, after which absolute hotspot motion is predicted from model outcome  
 607 (Doubrovine et al., 2012), an iterative process where the absolute plate motion is pro-  
 608 gressively modified to consider mantle motions predicted by the model. The SEIRF cou-  
 609 ples more, and independent constraints on absolute plate motion and mantle flow, and  
 610 thus provides many novel and independent ways to train numerical simulations of solid  
 611 Earth behavior (see also Ghelichkhan et al. (2024)). It is important to realize, however,  
 612 that such iteratively trained models, such with moving hotspots, are not independent  
 613 'reference frames' as basis for geodynamic interpretations, but rather geodynamic inter-  
 614 pretations themselves.

## 615 **5 Conclusion**

616 In this study, we introduce the Solid Earth Integrated Reference Frame (SEIRF)  
 617 that couples kinematic observations of plate-mantle interaction and solid Earth change.  
 618 With a relative plate model as basis, we started by constructing a mantle reference frame  
 619 by minimizing continent velocity, under the simple null hypothesis that horizontal am-  
 620 bient mantle motions are negligible. We then used this 'base' frame to predict independ-  
 621 ent parameters resulting from plate-mantle interaction. In the current version of the

SEIRF, these include geological expressions of mantle plumes (hotspots, kimberlites, and large igneous provinces) relative to the edges of large low shear velocity provinces in the deep mantle from where they might derive, absolute trench motions, net lithosphere rotation, and true polar wander (by comparing to a paleomagnetic reference frame). Future additions may include e.g. the positions of subducted slabs imaged in seismic tomography relative to the associated subduction zones in the plate model. We illustrate the following applications of the SEIRF:

1. The investigation of anomalous behavior of kinematic parameters using coupled, independent observations. Anomalous behavior of one parameter may be corroborated by others or exist in isolation, which may aid identifying which observations challenge the state-of-the-art, and which may result from artifacts.
2. Constraining relative motions in the mantle. We show here how we may compute relative motion between different surface expressions of plume-plate interactions and deep-mantle structure. To further develop the SEIRF as a tool to better understand geodynamic processes, we consider quantifying slab locations in the mantle as a key next step. The additions of slabs into this frame in the future would open the possibility of understanding relative motions between slabs and between slabs and plumes. The SEIRF thus essentially flips the classical view of mantle reference frames: it places observations of mantle motion into a plate tectonic reference frame.
3. Training numerical models of solid Earth dynamics. Similarly to previous attempts to reconcile hotspot records with dynamic models of mantle flow, the constraints integrated into the SEIRF may be used to iteratively train 3D numerical simulations of mantle convection. The SEIRF thereby integrates different approaches to constraining absolute plate motion into one coupled system of kinematic constraints with one common unknown: true absolute plate motion.

## Open Research Section

An updated version of the code published in Tetley et al. (2019) that we developed for the purposes of our paper, as well as the Python code needed to compute the data underlying the figures and to produce the figures is available on:

<https://github.com/StefaniaWagenaar/SEIRF.git>.

## Acknowledgments

Our paper benefited greatly from the TRM code of Michael Tetley on the Earthbyte Github, which we retrieved in 2023. We thank Lukas van der Wiel for support with the adaptation of the code to the Utrecht University High Performance Cluster.

## References

- Advokaat, E. L., & van Hinsbergen, D. J. (2024). Finding argoland: Reconstructing a microcontinental archipelago from the se asian accretionary orogen. *Gondwana Research*.
- Atkins, S., & Coltice, N. (2021, October). Constraining the Range and Variation of Lithospheric Net Rotation Using Geodynamic Modeling. *Journal of Geophysical Research: Solid Earth*, *126*. doi: 10.1029/2021JB022057
- Becker, T. (2008). Azimuthal seismic anisotropy constrains net rotation of the lithosphere. *Geophysical Research Letters*, *35*(5).
- Becker, T., Schaeffer, A., Lebedev, S., & Conrad, C. (2015). Toward a generalized plate motion reference frame. *Geophysical Research Letters*, *42*(9), 3188–3196.
- Besse, J., & Courtillot, V. (2002). Apparent and true polar wander and the geom-

- etry of the geomagnetic field over the last 200 myr. *Journal of Geophysical Research: Solid Earth*, 107(B11), EPM-6.
- 669 Bodur, Ö. F., & Flament, N. (2023). Kimberlite magmatism fed by upwelling above  
670 mobile basal mantle structures. *Nature Geoscience*, 16(6), 534–540.
- 671 Boschman, L. M., Van Hinsbergen, D. J., Langereis, C. G., Flores, K. E., Kamp,  
672 P. J., Kimbrough, D. L., ... Spakman, W. (2021). Reconstructing lost plates  
673 of the panthalassa ocean through paleomagnetic data from circum-pacific  
674 accretionary orogens. *American Journal of Science*, 321(6), 907–954.
- 675 Buffan, L., Jones, L. A., Domeier, M., Scotese, C. R., Zahirovic, S., & Varela, S.  
676 (2023). Mind the uncertainty: Global plate model choice impacts deep-time  
677 palaeobiological studies. *Methods in Ecology and Evolution*, 14(12), 3007–  
678 3019.
- 679 Burke, K. C., Steinberger, B., Torsvik, T. H., & Smethurst, M. A. (2008). Plume  
680 generation zones at the margins of large low shear velocity provinces on the  
681 core–mantle boundary. *Earth and Planetary Science Letters*, 265(1-2), 49–60.
- 682 Burke, K. C., & Torsvik, T. H. (2004). Derivation of large igneous provinces of  
683 the past 200 million years from long-term heterogeneities in the deep mantle.  
684 *Earth and Planetary Science Letters*, 227(3-4), 531–538.
- 685 Burke, K. C., & Wilson, J. T. (1976). Hot spots on the earth’s surface. *Scientific  
686 American*, 235(2), 46–59.
- 687 Butterworth, N., Talsma, A., Müller, R., Seton, M., Bunge, H.-P., Schuberth, B.,  
688 ... Heine, C. (2014). Geological, tomographic, kinematic and geodynamic  
689 constraints on the dynamics of sinking slabs. *Journal of Geodynamics*, 73,  
690 1–13.
- 691 Cao, X., Collins, A. S., Pisarevsky, S., Flament, N., Li, S., Hasterok, D., & Müller,  
692 R. D. (2024). Earth’s tectonic and plate boundary evolution over 1.8 billion  
693 years. *Geoscience Frontiers*, 101922.
- 694 Clennett, E. J., Holt, A. F., Tetley, M. G., Becker, T. W., & Faccenna, C. (2023,  
695 June). Assessing plate reconstruction models using plate driving force consistency  
696 tests. *Scientific Reports*, 13(1), 10191. doi: 10.1038/s41598-023-37117  
697 -w
- 698 Clennett, E. J., Sigloch, K., Mihalynuk, M. G., Seton, M., Henderson, M. A., Hos-  
699 seini, K., ... Müller, R. D. (2020). A quantitative tomotectonic plate recon-  
700 struction of western north america and the eastern pacific basin. *Geochemistry,  
701 Geophysics, Geosystems*, 21(8), e2020GC009117.
- 702 Conrad, C. P., & Behn, M. D. (2010). Constraints on lithosphere net ro-  
703 tation and asthenospheric viscosity from global mantle flow models and  
704 seismic anisotropy. *Geochemistry, Geophysics, Geosystems*, 11(5). doi:  
705 10.1029/2009GC002970
- 706 Cox, A., & Hart, R. B. (1991). *Plate tectonics: How it works*. John Wiley & Sons.
- 707 Domeier, M., Shephard, G. E., Jakob, J., Gaina, C., Doubrovine, P. V., & Torsvik,  
708 T. H. (2017). Intraoceanic subduction spanned the pacific in the late  
709 cretaceous–paleocene. *Science Advances*, 3(11), eaao2303.
- 710 Domeier, M., & Torsvik, T. H. (2019). Full-plate modelling in pre-jurassic time. *Ge-  
711 ological Magazine*, 156(2), 261–280.
- 712 Doubrovine, P. V., Steinberger, B., & Torsvik, T. H. (2012). Absolute plate motions  
713 in a reference frame defined by moving hot spots in the Pacific, Atlantic, and  
714 Indian oceans. *Journal of Geophysical Research: Solid Earth*, 117(B9). doi:  
715 10.1029/2011JB009072
- 716 Doubrovine, P. V., & Tarduno, J. A. (2008). Linking the late cretaceous to paleo-  
717 gene pacific plate and the atlantic bordering continents using plate circuits and  
718 paleomagnetic data. *Journal of Geophysical Research: Solid Earth*, 113(B7).
- 719 Duncan, R. A. (1981, April). Hotspots in the Southern Oceans — an absolute frame  
720 of reference for motion of the Gondwana continents. *Tectonophysics*, 74(1),  
721 29–42. doi: 10.1016/0040-1951(81)90126-8
- 722  
723

- 724 Duncan, R. A., & Richards, M. (1991). Hotspots, mantle plumes, flood basalts, and  
725 true polar wander. *Reviews of Geophysics*, *29*(1), 31–50.
- 726 Faccenna, C., Heuret, A., Funicello, F., Lallemand, S., & Becker, T. W. (2007). Pre-  
727 dicting trench and plate motion from the dynamics of a strong slab. *Earth and*  
728 *Planetary Science Letters*, *257*(1-2), 29–36.
- 729 Forsyth, D., & Uyeda, S. (1975, October). On the Relative Importance of the Driv-  
730 ing Forces of Plate Motion\*. *Geophysical Journal International*, *43*(1), 163–  
731 200. doi: 10.1111/j.1365-246X.1975.tb00631.x
- 732 Garnero, E. J. (2000). Heterogeneity of the lowermost mantle. *Annual Review of*  
733 *Earth and Planetary Sciences*, *28*(1), 509–537.
- 734 Ghelichkhan, S., Gibson, A., Davies, D. R., Kramer, S. C., & Ham, D. A. (2024).  
735 Automatic adjoint-based inversion schemes for geodynamics: reconstructing  
736 the evolution of earth’s mantle in space and time. *Geoscientific Model Develop-*  
737 *ment*, *17*(13), 5057–5086.
- 738 Goldreich, P., & Toomre, A. (1969). Some remarks on polar wandering. *Journal of*  
739 *Geophysical Research*, *74*(10), 2555–2567.
- 740 Gérard, M., Becker, T. W., Kaus, B. J. P., Faccenna, C., Moresi, L., & Husson, L.  
741 (2012). The role of slabs and oceanic plate geometry in the net rotation of the  
742 lithosphere, trench motions, and slab return flow. *Geochemistry, Geophysics,*  
743 *Geosystems*, *13*(4). doi: 10.1029/2011GC003934
- 744 Hassan, R., Müller, R. D., Gurnis, M., Williams, S. E., & Flament, N. (2016). A  
745 rapid burst in hotspot motion through the interaction of tectonics and deep  
746 mantle flow. *Nature*, *533*(7602), 239–242.
- 747 Kent, J. T. (1982). The fisher-bingham distribution on the sphere. *Journal of the*  
748 *Royal Statistical Society: Series B (Methodological)*, *44*(1), 71–80.
- 749 Konstantinovskaia, E. (2001). Arc–continent collision and subduction reversal in the  
750 cenozoic evolution of the northwest pacific: an example from kamchatka (ne  
751 russia). *Tectonophysics*, *333*(1-2), 75–94.
- 752 Lallemand, S., Heuret, A., & Boutelier, D. (2005). On the relationships between  
753 slab dip, back-arc stress, upper plate absolute motion, and crustal nature  
754 in subduction zones. *Geochemistry, Geophysics, Geosystems*, *6*(9). doi:  
755 10.1029/2005GC000917
- 756 Le Pichon, X., Jellinek, M., Lenardic, A., Şengör, A. C., & İmren, C. (2021). Pangea  
757 migration. *Tectonics*, *40*(6), e2020TC006585.
- 758 Le Pichon, X., Şengör, A. C., Jellinek, M., Lenardic, A., & İmren, C. (2023).  
759 Breakup of pangea and the cretaceous revolution. *Tectonics*, *42*(2),  
760 e2022TC007489.
- 761 Le Pichon, X., Şengör, A. M. C., & İmren, C. (2019). Pangea and the Lower Mantle.  
762 *Tectonics*, *38*(10), 3479–3504. doi: 10.1029/2018TC005445
- 763 Lin, Y.-A., Colli, L., & Wu, J. (2022). Nw pacific-panthalassa intra-oceanic sub-  
764 duction during mesozoic times from mantle convection and geoid models. *Geo-*  
765 *chemistry, Geophysics, Geosystems*, *23*(11), e2022GC010514.
- 766 Livermore, R., Vine, F., & Smith, A. (1984). Plate motions and the geomagnetic  
767 field—ii. jurassic to tertiary. *Geophysical Journal International*, *79*(3), 939–  
768 961.
- 769 Martin, C. R., Jagoutz, O., Upadhyay, R., Royden, L. H., Eddy, M. P., Bailey, E.,  
770 ... Weiss, B. P. (2020). Paleocene latitude of the kohistan–ladakh arc indi-  
771 cates multistage india–eurasia collision. *Proceedings of the National Academy*  
772 *of Sciences*, *117*(47), 29487–29494.
- 773 McKenzie, D. P. (1969). Speculations on the consequences and causes of plate mo-  
774 tions. *Geophysical Journal International*, *18*(1), 1–32.
- 775 Merdith, A. S., Williams, S. E., Collins, A. S., Tetley, M. G., Mulder, J. A., Blades,  
776 M. L., ... Müller, R. D. (2021, March). Extending full-plate tectonic models  
777 into deep time: Linking the Neoproterozoic and the Phanerozoic. *Earth-*  
778 *Science Reviews*, *214*, 103477. doi: 10.1016/j.earscirev.2020.103477



- 779 Morgan, W. J. (1972). Deep mantle convection plumes and plate motions. *AAPG*  
780 *bulletin*, *56*(2), 203–213.
- 781 Müller, R. D., Flament, N., Cannon, J., Tetley, M. G., Williams, S. E., Cao, X., ...  
782 Merdith, A. (2022, July). A tectonic-rules-based mantle reference frame since 1  
783 billion years ago – implications for supercontinent cycles and plate–mantle system  
784 evolution. *Solid Earth*, *13*(7), 1127–1159. (Publisher: Copernicus GmbH)  
785 doi: 10.5194/se-13-1127-2022
- 786 Müller, R. D., Royer, J.-Y., & Lawver, L. A. (1993, March). Revised plate motions  
787 relative to the hotspots from combined Atlantic and Indian Ocean hotspot  
788 tracks. *Geology*, *21*(3), 275–278. doi: 10.1130/0091-7613(1993)021<0275:  
789 RPMRTT>2.3.CO;2
- 790 Müller, R. D., Zahirovic, S., Williams, S. E., Cannon, J., Seton, M., Bower, D. J.,  
791 ... Gurnis, M. (2019). A Global Plate Model Including Lithospheric Deformation  
792 Along Major Rifts and Orogens Since the Triassic. *Tectonics*, *38*(6),  
793 1884–1907. doi: 10.1029/2018TC005462
- 794 O’Neill, C., Müller, D., & Steinberger, B. (2005). On the uncertainties in hot  
795 spot reconstructions and the significance of moving hot spot reference frames.  
796 *Geochemistry, Geophysics, Geosystems*, *6*(4). Retrieved 2024-03-14, from  
797 <https://onlinelibrary.wiley.com/doi/abs/10.1029/2004GC000784>  
798 (\_eprint: <https://onlinelibrary.wiley.com/doi/pdf/10.1029/2004GC000784>)  
799 doi: 10.1029/2004GC000784
- 800 Parsons, A. J., Sigloch, K., & Hosseini, K. (2021). Australian plate subduction is  
801 responsible for northward motion of the india-asia collision zone and 1,000  
802 km lateral migration of the indian slab. *Geophysical Research Letters*, *48*(18),  
803 e2021GL094904.
- 804 Rojas-Agramonte, Y., Kaus, B. J., Piccolo, A., Williams, I. S., Gerdes, A., Wong, J.,  
805 ... others (2022). Zircon dates long-lived plume dynamics in oceanic islands.  
806 *Geochemistry, Geophysics, Geosystems*, *23*(11), e2022GC010485.
- 807 Rose, I. R., Zhang, Y., & Swanson-Hysell, N. L. (2022). Bayesian paleomagnetic  
808 euler pole inversion for paleogeographic reconstruction and analysis. *Journal of*  
809 *Geophysical Research: Solid Earth*, *127*(10), e2021JB023890.
- 810 Schellart, W. P., Freeman, J., Stegman, D. R., Moresi, L., & May, D. (2007). Evo-  
811 lution and diversity of subduction zones controlled by slab width. *Nature*,  
812 *446*(7133), 308–311.
- 813 Schellart, W. P., Stegman, D. R., & Freeman, J. (2008, May). Global trench  
814 migration velocities and slab migration induced upper mantle volume  
815 fluxes: Constraints to find an Earth reference frame based on minimiz-  
816 ing viscous dissipation. *Earth-Science Reviews*, *88*(1), 118–144. doi:  
817 10.1016/j.earscirev.2008.01.005
- 818 Seton, M., Williams, S. E., Domeier, M., Collins, A. S., & Sigloch, K. (2023,  
819 March). Deconstructing plate tectonic reconstructions. *Nature Re-*  
820 *views Earth & Environment*, *4*(3), 185–204. Retrieved 2024-02-12, from  
821 <https://www.nature.com/articles/s43017-022-00384-8> (Number: 3  
822 Publisher: Nature Publishing Group) doi: 10.1038/s43017-022-00384-8
- 823 Sigloch, K., & Mihalynuk, M. G. (2013). Intra-oceanic subduction shaped the assem-  
824 bly of cordilleran north america. *Nature*, *496*(7443), 50–56.
- 825 Solomon, S. C., Sleep, N. H., & Richardson, R. M. (1975, August). On the Forces  
826 Driving Plate Tectonics: Inferences from Absolute Plate Velocities and In-  
827 traplate Stress. *Geophysical Journal International*, *42*(2), 769–801. doi:  
828 10.1111/j.1365-246X.1975.tb05891.x
- 829 Spakman, W., Chertova, M. V., van den Berg, A., & van Hinsbergen, D. J. (2018).  
830 Puzzling features of western mediterranean tectonics explained by slab drag-  
831 ging. *Nature Geoscience*, *11*(3), 211–216.
- 832 Stampfli, G. M., & Borel, G. (2002). A plate tectonic model for the paleozoic and  
833 mesozoic constrained by dynamic plate boundaries and restored synthetic

- 834 oceanic isochrons. *Earth and Planetary science letters*, 196(1-2), 17–33.
- 835 Steinberger, B. (2000). Plumes in a convecting mantle: Models and observations for  
836 individual hotspots. *Journal of Geophysical Research: Solid Earth*, 105(B5),  
837 11127–11152.
- 838 Steinberger, B., Seidel, M.-L., & Torsvik, T. H. (2017). Limited true polar wander as  
839 evidence that earth’s nonhydrostatic shape is persistently triaxial. *Geophysical*  
840 *Research Letters*, 44(2), 827–834.
- 841 Steinberger, B., & Torsvik, T. H. (2008, April). Absolute plate motions and true po-  
842 lar wander in the absence of hotspot tracks. *Nature*, 452(7187), 620–623. doi:  
843 10.1038/nature06824
- 844 Steinberger, B., & Torsvik, T. H. (2010). Toward an explanation for the present and  
845 past locations of the poles. *Geochemistry, Geophysics, Geosystems*, 11(6).
- 846 Tarduno, J. A., & Cottrell, R. D. (1997). Paleomagnetic evidence for motion of the  
847 hawaiian hotspot during formation of the emperor seamounts. *Earth and Plan-*  
848 *etary Science Letters*, 153(3-4), 171–180.
- 849 Tarduno, J. A., Duncan, R. A., Scholl, D. W., Cottrell, R. D., Steinberger, B., Thor-  
850 darson, T., ... others (2003). The emperor seamounts: Southward motion of  
851 the hawaiian hotspot plume in earth’s mantle. *Science*, 301(5636), 1064–1069.
- 852 Tetley, M. G., Williams, S. E., Gurnis, M., Flament, N., & Müller, R. D. (2019).  
853 Constraining Absolute Plate Motions Since the Triassic. *Journal of Geophysi-*  
854 *cal Research: Solid Earth*, 124(7), 7231–7258. doi: 10.1029/2019JB017442
- 855 Torsvik, T. H., Amundsen, H., Hartz, E. H., Corfu, F., Kuznir, N., Gaina, C., ...  
856 Jamtveit, B. (2013). A precambrian microcontinent in the indian ocean.  
857 *Nature geoscience*, 6(3), 223–227.
- 858 Torsvik, T. H., Burke, K. C., Steinberger, B., Webb, S. J., & Ashwal, L. D. (2010,  
859 July). Diamonds sampled by plumes from the core–mantle boundary. *Nature*,  
860 466(7304), 352–355. doi: 10.1038/nature09216
- 861 Torsvik, T. H., & Cocks, L. R. M. (2019, February). The integration of palaeo-  
862 magnetism, the geological record and mantle tomography in the loca-  
863 tion of ancient continents. *Geological Magazine*, 156(2), 242–260. doi:  
864 10.1017/S001675681700098X
- 865 Torsvik, T. H., Müller, R. D., Van der Voo, R., Steinberger, B., & Gaina, C. (2008).  
866 Global plate motion frames: Toward a unified model. *Reviews of Geophysics*,  
867 46(3). doi: 10.1029/2007RG000227
- 868 Torsvik, T. H., Smethurst, M. A., Burke, K. C., & Steinberger, B. (2006). Large ig-  
869 neous provinces generated from the margins of the large low-velocity provinces  
870 in the deep mantle. *Geophysical Journal International*, 167(3), 1447–1460.
- 871 Torsvik, T. H., Steinberger, B., Gurnis, M., & Gaina, C. (2010, March). Plate tec-  
872 tonics and net lithosphere rotation over the past 150My. *Earth and Planetary*  
873 *Science Letters*, 291(1), 106–112. doi: 10.1016/j.epsl.2009.12.055
- 874 Torsvik, T. H., van der Voo, R., Doubrovine, P. V., Burke, K., Steinberger, B., Ash-  
875 wal, L. D., ... Bull, A. L. (2014). Deep mantle structure as a reference frame  
876 for movements in and on the earth. *Proceedings of the National Academy of*  
877 *Sciences*, 111(24), 8735–8740.
- 878 Torsvik, T. H., Van der Voo, R., Preeden, U., Mac Niocaill, C., Steinberger, B.,  
879 Doubrovine, P. V., ... Cocks, L. R. M. (2012, September). Phanerozoic po-  
880 lar wander, palaeogeography and dynamics. *Earth-Science Reviews*, 114(3),  
881 325–368. doi: 10.1016/j.earscirev.2012.06.007
- 882 Vaes, B., & van Hinsbergen, D. J. (2024). Slow true polar wander around varying  
883 equatorial axes since 320 ma.
- 884 Vaes, B., Van Hinsbergen, D. J., & Boschman, L. M. (2019). Reconstruction of  
885 subduction and back-arc spreading in the nw pacific and aleutian basin: Clues  
886 to causes of cretaceous and eocene plate reorganizations. *Tectonics*, 38(4),  
887 1367–1413.
- 888 Vaes, B., van Hinsbergen, D. J. J., van de Lagemaat, S. H. A., van der Wiel,

- 889 E., Lom, N., Advokaat, E. L., . . . Langereis, C. G. (2023, October). A  
 890 global apparent polar wander path for the last 320 Ma calculated from  
 891 site-level paleomagnetic data. *Earth-Science Reviews*, *245*, 104547. doi:  
 892 10.1016/j.earscirev.2023.104547
- 893 van de Lagemaat, S. H., Cao, L., Asis, J., Advokaat, E. L., Mason, P. R. D.,  
 894 Dekkers, M. J., & van Hinsbergen, D. J. J. (2024, March). Causes of Cre-  
 895 taceous subduction termination below South China and Borneo: Was the  
 896 Proto-South China Sea underlain by an oceanic plateau? *Geoscience Fron-*  
 897 *tiers*, *15*(2), 101752. doi: 10.1016/j.gsf.2023.101752
- 898 van de Lagemaat, S. H., Kamp, P. J., Boschman, L. M., & Van Hinsbergen, D. J.  
 899 (2023). Reconciling the cretaceous breakup and demise of the phoenix plate  
 900 with east gondwana orogenesis in new zealand. *Earth-Science Reviews*, *236*,  
 901 104276.
- 902 van de Lagemaat, S. H., Van Hinsbergen, D. J., Boschman, L. M., Kamp, P. J., &  
 903 Spakman, W. (2018). Southwest pacific absolute plate kinematic reconstruc-  
 904 tion reveals major cenozoic tonga-kermadec slab dragging. *Tectonics*, *37*(8),  
 905 2647–2674.
- 906 Van der Meer, D., Torsvik, T., Spakman, W., Van Hinsbergen, D., & Amaru, M.  
 907 (2012). Intra-panthalassa ocean subduction zones revealed by fossil arcs and  
 908 mantle structure. *Nature Geoscience*, *5*(3), 215–219.
- 909 van der Meer, D. G., Spakman, W., van Hinsbergen, D. J. J., Amaru, M. L., &  
 910 Torsvik, T. H. (2010, January). Towards absolute plate motions con-  
 911 strained by lower-mantle slab remnants. *Nature Geoscience*, *3*(1), 36–40.  
 912 doi: 10.1038/ngeo708
- 913 van der Meer, D. G., van Hinsbergen, D. J. J., & Spakman, W. (2018, January).  
 914 Atlas of the underworld: Slab remnants in the mantle, their sinking history,  
 915 and a new outlook on lower mantle viscosity. *Tectonophysics*, *723*, 309–448.  
 916 doi: 10.1016/j.tecto.2017.10.004
- 917 van Hinsbergen, D. J., Kapp, P., Dupont-Nivet, G., Lippert, P. C., DeCelles, P. G.,  
 918 & Torsvik, T. H. (2011). Restoration of Cenozoic deformation in Asia and the  
 919 size of Greater India. *Tectonics*, *30*(5).
- 920 van Hinsbergen, D. J., & Schmid, S. M. (2012). Map view restoration of aegean-  
 921 west anatolian accretion and extension since the eocene. *Tectonics*, *31*(5).
- 922 van Hinsbergen, D. J., Torsvik, T. H., Schmid, S. M., Matenco, L. C., Maffione, M.,  
 923 Vissers, R. L., . . . Spakman, W. (2020). Orogenic architecture of the mediter-  
 924 ranean region and kinematic reconstruction of its tectonic evolution since the  
 925 triassic. *Gondwana Research*, *81*, 79–229.
- 926 Williams, S., Flament, N., Dietmar Müller, R., & Butterworth, N. (2015,  
 927 May). Absolute plate motions since 130 Ma constrained by subduction  
 928 zone kinematics. *Earth and Planetary Science Letters*, *418*, 66–77. doi:  
 929 10.1016/j.epsl.2015.02.026
- 930 Wilson, J. T. (1963). A possible origin of the hawaiian islands. *Canadian Journal of*  
 931 *Physics*, *41*(6), 863–870.
- 932 Wolf, J., & Long, M. D. (2023). Lowermost mantle structure beneath the central pa-  
 933 cific ocean: Ultralow velocity zones and seismic anisotropy. *Geochemistry, Geo-*  
 934 *physics, Geosystems*, *24*(6), e2022GC010853.
- 935 Zahirovic, S., Müller, R. D., Seton, M., & Flament, N. (2015, May). Tectonic speed  
 936 limits from plate kinematic reconstructions. *Earth and Planetary Science Let-*  
 937 *ters*, *418*, 40–52. doi: 10.1016/j.epsl.2015.02.037